REDOX EFFECTS ON WETLAND MICROBIAL METABOLIC COMPOSITION

By

Colin G. Finlay

July 2023

Director of Thesis: Ariane L. Peralta, PhD

Major Department: Department of Biology

ABSTRACT

Wetlands provide valuable ecosystem functions including nutrient recycling, carbon storage, flood mitigation, and habitat in support of biodiversity. However, land use change and climate change continue to threaten wetland ecosystems. Climate change is predicted to increase rates of sea-level rise and increase frequency of storm surges. Therefore, we need to better understand how saltwater intrusion and flooding influence coastal wetlands. In a previous experiment, a soil mesocosm approach was used to examine how hydrology (wet, dry, interim) and plant presence (with or without plants) influenced wetland soils sampled from varying hydrologic histories (wet, dry, interim) in a restored, coastal wetland. After eight weeks of hydrologic manipulation, 16S rRNA amplicon sequencing and shotgun metagenomic sequencing were performed to characterize the microbial communities and greenhouse gas concentrations were measured to assess microbial function. Soil redox potential and soil physicochemical properties were also measured. Previous results showed that plant presence decreased greenhouse gas concentrations even in flooded conditions, and hydrology (history and contemporary treatment) altered wetland soil microbial community structure and the composition of carbohydrate metabolic genes. Genes involved in

methanogenesis, and aerobic respiration, also differed in composition across hydrologic histories. In this study, we address the questions (1) how do hydrologic and plant related redox shifts relate to the composition of metabolic genes involved in sulfur/iron cycling and (2) how do patterns of iron-sulfur metabolic composition relate to carbon and nitrogen metabolic composition and greenhouse gas production? We hypothesize that the most reducing conditions (i.e., prolonged flooded, no plants) modify anaerobic metabolisms in similar ways. We predict that (i) in oxidizing conditions (dry and/or plant presence), functional gene composition of sulfate reduction will not correlate to the gene composition of iron reduction, and (ii) in reducing conditions (i.e., wet and/or plant absence), functional gene composition of sulfate reduction will correlate to patterns in iron reduction metabolic genes. In addition, iron and sulfur metabolic gene composition will contribute to carbon dioxide production while competing with methanogenesis. Results revealed that hydrologic treatment impacted assimilatory sulfate reduction gene composition, while hydrologic history impacted dissimilatory sulfate reduction composition. Hydrologic history significantly affected total iron active gene composition and iron reduction gene composition. We also identified correlations between sulfate reduction and iron reduction, and sulfate reduction and iron reduction compositions explained variation in carbon dioxide and methane. These results demonstrate the role of historical hydrology, saltwater exposure, and soil iron in shaping microbial community responses to future changes in hydrology and plant cover. Salinization events and changing precipitation patterns impact soil redox dynamics by altering sulfate and oxygen availability, and challenge estimates of biogenic greenhouse gas emissions. Therefore, a better understanding of microbial community responses to hydrologic manipulations, plant presence/absence, and soil physicochemistry will inform wetland greenhouse gas emissions predictions and management strategies (e.g., plant presence and hydrologic flows).

REDOX EFFECTS ON WETLAND MICROBIAL METABOLIC COMPOSITION

A Thesis

Presented to the Faculty of the Department of Biology

East Carolina University

In Partial Fulfillment of the Requirements for the Degree

Master of Science in Biology

By

Colin G. Finlay

July 2023

Director of Thesis: Ariane L. Peralta, PhD
Thesis Committee Members:
Erin K. Field, PhD
John P. Hoben, PhD

TABLE OF CONTENTS

LIST OF TABLES

LIST OF FIGURES

INTRODUCTION

In coastal wetlands, saltwater inundation may impose flooded conditions and the influx of terminal electron acceptors (TEAs) such as sulfate (SO_4^{2-}) (Herbert et al., 2015; Hopfensperger et al., 2014). Flooding alters the terminal electron acceptor pool, by decreasing soil oxygen levels (Kozlowski, 1984), and saltwater intrusion from marine sources introduces sulfate to the ecosystem (Ardón et al., 2013; Herbert et al., 2015; Schoepfer et al., 2014). The combined impacts of flooding and SO_4^{2-} addition on wetland ecosystem function are poorly understood, in part because varying environmental characteristics, especially soil iron, could buffer the effects of SO_4^{2-} intrusion (Schoepfer et al., 2014). With climate change predicted to increase rates of sea-level rise and increase frequency of storm surges from more intense tropical storms, we need to better understand how the combined saltwater intrusion and flooding environmental stressors influence coastal wetlands (Pörtner et al., 2022).

To harvest energy through respiration, microorganisms oxidize organic or inorganic substances, and transfer the electrons through electron transport chains, to ultimately reduce a TEA (Burgin et al., 2011). Oxygen (O_2) is used as a TEA in aerobic respiration (reviewed in Glass et al., 2022). In the absence of O_2, a variety of other TEAs may be used in anaerobic respiration, including nitrate (NO_3^-), ferric iron (Fe(III)), SO_4^{2-}, and carbon dioxide (CO_2) (Wang et al., 2017). In common with these respiratory (i.e., dissimilatory) processes, assimilatory processes also involve oxidation-reduction (redox) reactions (Burgin et al., 2011). The availability of specific reductants (e.g., organic matter), and specific oxidants (e.g., TEAs like O_2) modulate both dissimilatory and assimilatory processes (Burgin et al., 2011). The overall propensity of a soil environment to reduce or oxidize is called soil redox potential and integrates relative levels of reductants and oxidants within the soil (Burgin et al., 2011). In this study, we also refer to the overall oxidation-reduction propensity of the environment as “redox status”.

Soil redox potential influences microbial community structure and function (DeAngelis et al., 2010; Peralta et al., 2014). As soil microbes are major drivers of biogeochemical cycles, soil redox potential affects microbial metabolic capacity, ultimately influencing transformations of carbon (C), nitrogen (N), sulfur (S), and iron (Fe) at the ecosystem level (Crowther et al., 2019; Falkowski et al., 2008; Schlesinger et al., 2011; Wang et al., 2017). While the prediction of microbial metabolic diversity is inferred by taxonomic approaches, characterizing microbial metabolic diversity by examining genetic potential (e.g., shotgun metagenomics) provides a more direct evaluation of functional potential (Quince et al., 2017; Toole et al., 2021). To further improve prediction of microbial functions, it is critical to understand how changing environmental conditions directly affect soil redox conditions.

Dynamic wetland hydrologic conditions modify soil redox status (Peralta et al., 2014). Flooding of soils fills pore space, thereby restricting access to atmospheric O_2 (Pezeshki and DeLaune, 2012). This creates suboxic/anoxic conditions, requiring alternative TEAs to be used in anaerobic respiration (Patrick Jr. and Jugsujinda, 1992; RoyChowdhury et al., 2018). Based on the hydrologic regime of a wetland, soils therein may experience fluctuating wet/dry conditions, as well as prolonged inundation or dry down (DeAngelis et al., 2010; Peralta et al., 2014; RoyChowdhury et al., 2018).

In addition to dynamic hydrology, human activities modify biogeochemical cycles. For example, watersheds accumulate N via human activities, and this N may be loaded in coastal wetlands via hydrologic flows and atmospheric deposition (Chilton et al., 2021; Conley et al., 2009). The incoming N may be in the form of NO_3^- or converted to NO_3^- by internal microbial processing (e.g., nitrification, $NH_4^+ \rightarrow NO_3^-$) (Kuypers et al., 2018). Since NO_3^- is an efficient TEA, it is used in facultative anaerobic respiration, which is a common metabolism observed in

fluctuating oxic/anoxic conditions (Wallenstein et al., 2006). In addition, saltwater intrusion events can increase soil and porewater SO_4^{2-} concentrations (Herbert et al., 2018). Then, SO_4^{2-}-reducing microorganisms (SRM) produce sulfide which binds with reduced Fe to form FeS (Schoepfer et al., 2014). This buffering of seawater SO_4^{2-} is therefore dependent on the activity of SRM and Fe reducing microorganisms (FeRM), as well as the existing soil Fe concentrations (Schoepfer et al., 2014).

While human activities influence biogeochemical cycles, cross-kingdom interactions between plants and microorganisms also have important consequences for soil redox activity. Plants alter soil redox potential by delivering O_2 to the rhizosphere, and transporting CO_2 and methane (CH_4) from the rhizosphere to the atmosphere (Colmer, 2003). Plant root O_2 release can buffer the effects of flooding on soil aeration (Cook and Knight, 2003; Koop-Jakobsen and Wenzhöfer, 2015; Kozlowski, 1984). While hydrologic status can be variable over time, plants impose a more constant influence on soil redox conditions (Koop-Jakobsen and Wenzhöfer, 2015).

The biogeochemical cycles of C, N, Fe, and S are not isolated, but instead, closely linked. For example, NO_3^- reduction can be coupled to sulfide oxidation (Burgin and Hamilton, 2008). The oxidation of organic C is coupled to reductions of NO_3^-, Fe(III), and SO_4^{2-} (Burgin et al., 2011). The microbial N cycle forms an interconnected network, with many reactions dependent on availability of C, Fe, and S (Kuypers et al., 2018). Therefore, to understand the cycling of any one element, it is essential to consider the relevant coupled cycles and environmental controls on the nutrient cycling network.

Past work on saltwater intrusion and iron-sulfur buffering was conducted at the Timberlake Observatory for Wetland Restoration (TOWeR) (Schoepfer et al., 2014). The TOWeR site is prone to seasonal saltwater intrusion, which introduces SO_4^{2-} to Fe-rich soils (Ardón et al., 2013; Lamers

et al., 2013; Schoepfer et al., 2014). Both the SO_4^{2-} and Fe can be microbially reduced to sulfide and ferrous iron (Fe(II)), respectively (Lamers et al., 2013; Schoepfer et al., 2014; Weber et al., 2006). The sulfide may be toxic to salinity-naïve ecosystems, but can readily bind Fe(II) to create FeS, which is non-toxic and relatively non-bioavailable (Lamers et al., 2013; Schoepfer et al., 2014). Schoepfer and colleagues (2014) found that the pool of reduced Fe in TOWeR soils is sufficient to sequester sulfide from seasonal saltwater incursion into FeS, but as sea-level rise accelerates soil sulfidization, toxic sulfide levels may accumulate in the future.

The extent to which future sulfidization (due to saltwater incursion) will modify wetland microbial community structure and function is unknown. Specifically, it is unclear how wetland microbes that participate in S cycling might respond to flooding/drought, and changes in plant cover. This study addressed the questions (1) how do soil Fe and S concentrations interact with altered redox states (hydrology and plants) and microbial community composition of SO_4^{2-} reduction genes? and (2) how do these Fe-S metabolic dynamics relate to greenhouse gas (GHG) emissions, mediated by carbon/nitrogen metabolism? We hypothesize that the most reducing conditions (i.e., prolonged flooded, no plants) modify anaerobic metabolisms in similar ways and predict that (i) in oxidizing conditions (dry and/or plant presence) SO_4^{2-} reduction and Fe reduction will not be linked/coupled. Coupled here means a significant correlation between Bray-Curtis distance matrices of SO_4^{2-} reduction and Fe reduction, as determined by Mantel Test. We also predict that (ii) in reducing conditions (wet and/or plant absence) coupling between SO_4^{2-} reduction and Fe reduction will be observed, and these processes will contribute to CO_2 production (fit with CO_2 concentrations using envfit) while competing with methanogenesis (observed as negative relationship with methanogenic functional genes and CH_4 concentrations).

METHODS

Sampling and Mesocosm Experimental Design

On April 1, 2016, soil samples were collected from the Timberlake Observatory for Wetland Restoration (TOWeR) located in the Albemarle Peninsula in Tyrell County, North Carolina, USA (35°54'22" N, 76°09'25" W). The site is connected to the Albemarle Sound via the Little Alligator River, with potential for saltwater incursion. Across the sampling area, the position of the water table creates a hydrologic gradient, with sites categorized as dry (upland), wet (saturated), and interim (transition dry/wet) (Hopfensperger et al., 2014).

Soil blocks collected from the three sites within TOWeR (dry, wet, interim) were used to set up a mesocosm experiment. Soil history was determined by water table levels at the time of collection (dry = 20 cm, interim = 10 cm, and wet = 0 cm below surface level). Six intact soil blocks (25 cm x 25 cm x 20 cm) from each of the three hydrologic histories were contained in dark plastic containers of the same dimensions. Each block was then divided in half by a root screen (20 μm stainless steel mesh), and plants were allowed to grow on one side of the screen and removed (above- and belowground) on the other side of the screen to create "plant" and "no plant" treatments. Polyvinyl chloride (PVC) collars were installed in each mesocosm as a base for GHG sampling.

Hydrologic treatments were started two weeks after beginning plant treatments and installing PVC collars. To manipulate hydrology within the mesocosm, vinyl tubing was inserted 3 cm from the bottom of the mesocosm container on each side and connected to a 1 L water bottle. Water levels inside the mesocosm were maintained by filling the 1 L bottle to the desired height using rainwater collected from a cistern. Mesocosms exposed to wet conditions were flooded and maintained at maximum container height (18 cm). Mesocosms exposed to dry conditions were

maintained at a 5 cm water level. Interim hydrologic treatment fluctuated between flooded and dry conditions every two weeks, starting with a wet treatment, and ending with a dry treatment. Experimental treatment lasted eight weeks, with 36 mesocosms evenly representing three levels of hydrologic history (dry, wet, interim), two levels of plant treatment (plant, no plant), and three levels of hydrologic treatment (dry, wet, interim) in a factorial experimental design.

Measuring Greenhouse Gases

In situ GHG measurements began two weeks after hydrologic treatments were established, then measured every two weeks for a total of five sampling events. GHG concentrations were analyzed using a Shimazdu gas chromatograph (GC-2014) fitted with an electron capture detector to detect nitrous oxide (N_2O) and flame ionization detector with methanizer to measure CH_4 and CO_2. Concentrations of GHGs after 30 minutes of collection (with chambers attached) were used in analyses.

Amplicon and Shotgun Metagenomic Sequencing

Based on amplicon sequencing, we identified a subset of samples representing the most distinct microbial communities for shotgun metagenomic sequencing. Briefly, we chose a set of baseline (before hydrologic/plant treatment) and post-flooding/drying treatment samples. We sourced mesocosm baseline conditions from relatively drier field locations (water level at about -20 cm, n = 4) and relatively wetter plots (water level at about 0 cm, n = 4). At the end of the 8-week experiment, we selected a subset of samples from the hydrologic treatments (prolonged drying or wetting only) and plant treatments (presence or absence of vegetation) (n = 16). After genomic DNA extraction using the Qiagen DNeasy PowerMax soil kit, samples were sent to the U.S. Department of Energy (DOE) Joint Genome Institute (JGI) for sequencing and analysis (GOLD study ID Gs0142547 and NCBI BioProject accession number PRJNA641216). Bin

methods in the IMG pipeline (MetaBAT version 2.12.1, CheckM v1.0.12, GTDB database release 86, GTDB-tk version v0.2.2) were used to curate 14 medium- to high-quality bins from the metagenomes. Medium-quality bins have at least 50% completion, and less than 10% contamination. High quality bins have greater than 90% completion, less than 5% contamination, the presence of 23S, 16S, and 5S rRNA genes, and at least 18 tRNA genes (Bowers et al., 2017). Description of sample processing and metagenomic sequencing can be found in Peralta et al. 2020 (Peralta et al., 2020).

From the metagenomes, we curated functional gene sets using IMG/M's integrated Kyoto Encyclopedia of Genes and Genomes (KEGG) module list (Chen et al., 2017). For statistical analyses, we focused on the following four functional gene sets associated with biogenic GHG concentrations of N_2O, CH_4, and CO_2: (1) Denitrification (KEGG Module M00529), (2) Methanogen (M00617), (3) Central Carbohydrate Metabolism (M00001-M00011, M00307-M00309, M00580, and M00633), and (4) Prokaryotic Cytochrome C Oxidase (CcO) (M00155). For S cycling, we analyzed the following KEGG modules: Assimilatory Sulfate Reduction (M00176), Dissimilatory Sulfate Reduction (M00596), Thiosulfate Oxidation by SOX Complex (M00595), and Sulfate-Sulfur Assimilation (M00616). We also analyzed KEGG module M00530: Dissimilatory Nitrate Reduction to Ammonia (DNRA).

The IMG/M, and publicly available databases in general, have limited options for Fe gene analysis. From IMG/M's integrated TIGRFAM tool, we analyzed two genes putatively involved in Fe reduction: decaheme c-type cytochrome, OmcA/MtrC family (TIGR03507) and decaheme-associated outer membrane protein, MtrB/PioB family (TIGR03509). These two genes were analyzed together as one "module", analogous to collections of KEGG Orthologs (KOs) within each KEGG Module.

For further Fe gene analysis, we analyzed all metagenomes using FeGenie, a hidden Markov model (HMM) tool designed for the identification of Fe genes and Fe gene neighborhoods (Garber et al., 2020). Complete nucleotide assemblies (FNA files) for each metagenome were downloaded from IMG/MER, then searched using FeGenie's custom HMM scripts. Bitscores greater than the bitscore cuttoff were counted as positive "hits" for a given Fe gene. Counts of gene hits were totaled within each of FeGenie's gene categories:

1. iron acquisition:
    a. iron transport
    b. heme transport
    c. heme oxygenase
    d. siderophore synthesis
    e. siderophore transport
    f. siderophore transport potential
2. iron gene regulation
3. iron oxidation
4. possible iron oxidation and possible iron reduction
5. probable iron reduction
6. iron reduction
7. iron storage
8. magnetosome formation

Counts within each FeGenie category were then converted to relative abundance (relative to total Fe gene counts as determined by FeGenie), and relative abundance matrices were then converted to Bray-Curtis distance matrices. Functional gene counts within each respective KEGG

Module and TIGRfam "module", followed a similar process: conversion of counts to relative abundance (relative to module total counts), and conversion of relative abundance matrices to Bray-Curtis matrices.

Measuring Integrated Soil Redox Status

We measured soil redox status at the beginning and end of the hydrologic experiment using Indicator of Reduction in Soils (IRIS) tubes (InMass Technologies; Jenkinson and Franzmeier, 2006) (Fig. S1A). The IRIS tubes are constructed from 1/2" schedule 40 PVC pipe coated in iron oxide (Fe(III)) paint (Rabenhorst, 2008). When exposed to oxidative conditions, Fe(III) is visible as an orange-red paint; but when exposed to anoxic conditions, Fe(III) is reduced to Fe(II) which dissolves in solution and appears as a clearing (white) on the tube (Jenkinson and Franzmeier, 2006; Rabenhorst, 2008). At the beginning of the experiment, two IRIS tubes (12 cm depth) were installed in each mesocosm: one on the plant side and one on the bare soil side. The IRIS tubes were incubated in mesocosm conditions for two weeks before removal and analysis. After we removed the IRIS tube, a non-coated PVC pipe was used to fill the hole. Two weeks prior to the end of the experiment, the non-coated PVC pipe was removed and replaced with a new IRIS tube to measure soil redox status at the end of the experiment.

To measure redox status integrated over two weeks, we quantified the surface area of Fe(III) paint removed from IRIS tubes using ImageJ software (v1.48, (Schneider et al., 2012)). First, we imaged the entire tube by taking four pictures and then stitched the photo into a composite using GIMP2 (v2.8.14, https://gimp.org/) photo editing software. Next, we identified areas of artificial paint removal, that is scratches from installing or removing tubes, and manually filled these pixels. Then, using ImageJ software (v1.48, (Schneider et al., 2012)), we converted all colored pixels to black. We compared the number of white pixels to total pixels to determine the

percent of paint removed. Interpretation of redox status is based on the percent paint removed from a 10 cm section of tubing and summarized as follows: 0% not reducing, 1-5% probably not reducing, 5-10% possibly reducing, 10-25% and >25% definitely reducing (Rabenhorst, 2008).

Measuring Soil Factors

Soil proprieties were determined from soils collected during the destructive sampling of mesocosms at the end of the experiment. A sample of air-dried soil from each mesocosm was sent to Waters Agricultural Laboratories, Inc. (Warsaw, NC) and analyzed for pH, phosphorus, potassium, magnesium, sulfur, manganese, iron, and humic matter, using standard Mehlich III methods (Mehlich, 1984).

Statistical Analyses

All statistical analyses were performed in the R statistical environment (RStudio 2023.03.1+446, Rv4.3.0) (R Core Team, 2023). We examined beta diversity by visualizing bacterial community responses to hydrologic history (field conditions), hydrologic treatment (contemporary dry/wet treatments), and plant presence/absence using principal coordinates analysis (PCoA) of bacterial community composition based on Bray-Curtis dissimilarity. We also used PCoA to visualize beta diversity of functional gene categories, separating points by hydrologic history, hydrologic treatment, plant presence/absence, and baseline (sampled before beginning hydrologic and plant treatments). We used permutational multivariate analysis of variance (PERMANOVA) to determine differences between bacterial communities among hydrologic history, hydrologic treatment, and plant presence. Hypothesis testing using PERMANOVA was performed using the vegan::adonis function (Oksanen et al., 2022). Finally, soil parameters and GHG concentrations were compared against bacterial community and functional patterns (based on Bray-Curtis dissimilarity) using the vegan::envfit function (Oksanen

et al., 2022). Soil parameters with $P < 0.05$ were represented on the PCoA plot of 16S rRNA community composition as vectors scaled by their correlation to microbial community patterns. The GHG concentrations and soil parameters with envfit $P < 0.05$ were plotted as vectors, scaled by their correlation, on PCoA plots of functional gene composition. Distance-based partial least squares regression (DBPLSR) was used to measure relationships between Bray-Curtis distance matrices and GHG concentrations.

We conducted a series of Mantel tests to measure correlations between Bray-Curtis distance matrices. We assessed the potential for NO_3^--driven SO_4^{2-} production by testing the distance matrix correlations between the composition of NO_3^- reduction pathways (denitrification and DNRA) and the composition of thiosulfate oxidation by the SOX complex. We conducted a Mantel test for each respective NO_3^- reduction pathway (denitrification and DNRA) correlated to thiosulfate oxidation by the SOX complex. We ran a series of Mantel tests for pairs of SO_4^{2-} reduction and Fe reduction distance matrices: Fe reduction ~ SO_4^{2-} reduction (assimilatory and dissimilatory), Fe reduction ~ assimilatory SO_4^{2-} reduction, and Fe reduction ~ dissimilatory SO_4^{2-} reduction. To investigate correlations between SO_4^{2-} and Fe reduction under different hydrological conditions, the SO_4^2 reduction (assimilatory and dissimilatory) and Fe reduction modules were subset by hydrologic history (wet or dry) and hydrologic treatment (wet or dry). We evaluated the strength of Mantel r correlations between pairs of SO_4^{2-} reduction and Fe reduction distance matrices within each hydrologic condition (e.g., wet hydrologic history) and used a statistical cutoff of $P < 0.05$.

Data Availability

All code and data used in this study are in a public GitHub repository (https://github.com/colfin/WetlandMesocosm_GHG_Timberlake), and metagenome sequence files can be found at NCBI SRA BioProject ID PRJNA641216.

RESULTS

Using an experimental wetland mesocosm approach, we tested the following hypotheses: (i) in oxidizing conditions (dry and/or plant presence) SO_4^{2-} reduction and Fe reduction will not be linked/coupled, where coupled means a significant correlation between Bray-Curtis distance matrices of SO_4^{2-} reduction and Fe reduction; and (ii) in reducing conditions (wet and/or plant absence) coupling between SO_4^{2-} reduction and Fe reduction will be observed, and these processes will contribute to CO_2 production (fit with CO_2 concentrations using envfit) while competing with methanogenesis (observed as negative relationship with methanogenic functional genes and CH_4 concentrations).

Sulfur Functional Genes

We measured how hydrology and plant presence influenced metabolic composition of sulfur cycling genes. Hydrologic treatment strongly influenced the composition of SO_4^{2-}-S assimilation (PERMANOVA, $F_{1, 23} = 3.917$, $R^2 = 0.144$, $P = 0.008$; Table S5) and assimilatory SO_4^{2-} reduction functional genes (PERMANOVA, $F_{1, 23} = 4.111$, $R^2 = 0.156$, $P = 0.013$; Table S5). The response of SO_4^{2-}-S assimilation (envfit, $R^2 = 0.285$, $P = 0.032$, Figure 5B) and assimilatory SO_4^{2-} reduction gene composition correlated to redox status measured as the percent paint removed from IRIS tubes (envfit, $R^2 = 0.301$, $P = 0.027$, Figure 5A). Hydrologic history strongly influenced the compositions of dissimilatory SO_4^{2-} reduction (PERMANOVA, $F_{1, 23} = 10.397$, $R^2 = 0.316$, $P = 0.001$; Table S5) and thiosulfate oxidation by the SOX complex (PERMANOVA, $F_{1, 23} = 6.547$, $R^2 = 0.243$, $P = 0.009$; Table S5). The combination of assimilatory and dissimilatory SO_4^{2-} reduction differed in composition according to hydrologic history and treatment (PERMANOVA, history: $F_{1, 23} = 2.830$, $R^2 = 0.108$, $P = 0.030$, treatment: $F_{1, 23} = 2.906$, $R^2 = 0.111$, $P = 0.026$; Table S5). PCoA of SO_4^{2-} reduction (assimilatory and dissimilatory) correlated significantly with percent

soil moisture (envfit, $R^2 = 0.298$, $P = 0.023$; Figure 8C), supporting the importance of hydrology in SO_4^{2-} reduction gene composition identified by PERMANOVA (Table S5).

Nitrate-Driven Sulfate Production

To evaluate linkages between NO_3^- reduction and sulfide oxidation, we measured the extent to which metabolic composition of NO_3^- reduction pathways (denitrification and DNRA) related to thiosulfate oxidation. Results showed that DNRA was significantly correlated to thiosulfate oxidation by SOX complex ($R = 0.196$, $P = 0.0499$; Table S1), but denitrification was not correlated to thiosulfate oxidation by SOX complex ($R = 0.117$, $P = 0.170$; Table S1).

Iron Functional Genes

The composition of all Fe-active genes, and the composition of Fe reduction genes, were used to evaluate the response of Fe cycling communities from different hydrologic histories to flooding/drying and plant presence/absence. Hydrologic history influenced the composition of all Fe genes identified by FeGenie (PERMANOVA: $F_{1, 23} = 4.173$, $R^2 = 0.185$, $P = 0.031$; Table S5). The composition of the subset of Fe reduction genes identified by FeGenie also diverged according to history (PERMANOVA: $F_{1, 23} = 3.358$, $R^2 = 0.132$, $P = 0.004$; Table S5), while the composition of Fe reduction genes based on TIGRFAMS mtrBC differed by plant presence/absence and treatment (PERMANOVA, plant: $F_{2, 23} = 9.967$, $R^2 = 0.335$, $P = 0.002$, treatment: $F_{1, 23} = 19.012$, $R^2 = 0.319$, $P = 0.0002$; Table S5).

Sulfate Reduction and Iron Reduction

The functional groups SRM and FeRM produce sulfide and Fe(II) respectively, which can then form FeS and sequester toxic sulfide (Schoepfer et al., 2014). Previous work found a relationship between SO_4^{2-} reduction and Fe reduction rates in TOWeR soil (Schoepfer et al., 2014). In this study, we observed a significant correlation between the composition of functional

genes associated with Fe reduction and assimilatory SO_4^{2-} reduction (Mantel r = 0.222, P = 0.008; Table S1). Similarly, results showed a significant correlation between functional gene composition of Fe reduction and dissimilatory SO_4^{2-} reduction (Mantel r = 0.313, P = 0.006; Table S1). However, results showed no correlation when assimilatory and dissimilatory SO_4^{2-} reduction were combined into a single module and compared to Fe reduction (Mantel r = 0.064, P = 0.249; Table S1).

Then, we assessed correlations between SO_4^{2-} and Fe reduction under different hydrologic conditions. In the wet history, dry history, and dry treatment, there were no significant correlations between SO_4^{2-} reduction and Fe reduction (Table S2). In the wet treatment, there was a significant correlation between functional gene composition of SO_4^{2-} reduction and Fe reduction (Mantel r = 0.360, P = 0.010; Table S2).

Results revealed linkages between SO_4^{2-} and Fe reduction modules and carbon losses via GHG production. The composition of assimilatory SO_4^{2-} reduction functional genes significantly correlated with mg CO_2-C m^{-2} (envfit, R^2 = 0.256, P = 0.042; Figure 5B), and percent paint removed from IRIS tubes (envfit, R^2 = 0.301, P = 0.027; Figure 5B). The mg CO_2-C m^{-2} envfit vectors pointed toward samples from dry treatments, and the percent paint removed vector pointed in the opposite direction, toward samples from wet treatments (Figure 5B). We further investigated the relationship between assimilatory SO_4^{2-} reduction and CO_2 concentrations. Based on DBPLSR analyses, the variation in assimilatory SO_4^{2-} reduction gene composition explained 82.8% of variation in CO_2 at start of the experiment (adjusted R^2 for Components 1 and 2; Table S3). This relationship weakened by end of experiment, with assimilatory SO_4^{2-} reduction gene composition only explaining 28.28% of CO_2 variation (Components 1 and 2; Table S3).

At the end of the 8-week experiment, both dissimilatory SO_4^{2-} reduction and Fe reduction significantly correlated with mg CH_4-C m^{-2}, identified by PCoA with envfit (Figure 6C, Figure 8D). Based on DBPLSR, the percent of variation in mg CH_4-C m^{-2} explained by dissimilatory SO_4^{2-} reduction doubled from the Week 0 to Week 8 (adjusted $R^2_{Week\ 0}$ = 30.60, adjusted $R^2_{Week\ 8}$ = 61.738, based on Components 1 and 2; Table S4). Similarly, the percent of variation in mg CH_4-C m^{-2} explained by Fe reduction also increased by 2-fold from Week 0 to Week 8 (adjusted $R^2_{Week\ 0}$ = 39.48, adjusted $R^2_{Week\ 8}$ = 87.150, based on Components 1 and 2; Table S4).

Metagenome Bins

Bin methods in the IMG pipeline resulted in 14 medium- to high-quality metagenome bins (Table 2). Except for one bin attributed to an Archaeal lineage (*Candidatus* Nitrosotalea devanaterra), all other bins were identified as bacterial taxa (Table 2). The bins were sourced from varying hydrologic histories, hydrologic treatments, and plant presence/absence treatments. Due to relatively few resolved microbial taxa, we did not conduct further analyses.

DISCUSSION

Soil Fe availability, hydrologic conditions, and plant-microbe interactions mediate the impacts of sea-level rise on coastal freshwater wetlands (Ardón et al., 2013; Herbert et al., 2015; Schoepfer et al., 2014). In this study, we used an experimental mesocosm approach to examine the effects of hydrologic conditions and plant presence/absence on soils sourced from varying hydrologic histories (wet and dry). We found that hydrologic history (wet vs dry) influenced the composition of genes involved in dissimilatory SO_4^{2-} reduction, thiosulfate oxidation, and Fe reduction. The 8-week hydrologic manipulation also modified the community composition of assimilatory SO_4^{2-} reduction genes and resulted in correlated SO_4^{2-} reduction and Fe reduction gene compositions in the wet hydrologic treatment. The S and Fe gene modules were linked with C and N cycling; specifically, DNRA and thiosulfate oxidation gene compositions correlated, and SO_4^{2-} reduction and Fe reduction gene compositions explained variation in CO_2 and CH_4 concentrations. These results indicate that historical conditions strongly influence the magnitude of soil microbial community responses to contemporary changes in hydrologic conditions and plant cover.

Past and Current Hydrologic Changes Influence Sulfur Functional Genes

The influence of hydrologic conditions, both historical and during the 8-week hydrologic treatments, was evident in S-related gene modules. The community-level compositions of SO_4^{2-}-S assimilation and assimilatory SO_4^{2-} reduction genes both differed by hydrologic treatment, while the compositions of dissimilatory SO_4^{2-} reduction and thiosulfate oxidation by the SOX complex both differed by hydrologic history (Table S5). The composition of SO_4^{2-} reduction functional genes (assimilatory and dissimilatory) correlated with the percent soil moisture (Figure 8C). This relationship revealed the importance of hydrology in SO_4^{2-} reduction gene composition (Table S5).

The influence of hydrologic history on S metabolism at this coastal wetland is potentially two-fold: the introduction of SO_4^{2-} via saltwater intrusion, and the reducing conditions found in waterlogged soils (in wet history), compared to more oxidizing conditions likely found in drier conditions (at a greater elevation above the water table). Ardón and colleagues (2013) found evidence of saltwater incursion via surface water at TOWeR. There is potential for drought-induced saltwater incursion at this site, where the surrounding estuary's salinity increases during drought, and winds or tides transport the brackish water upstream to TOWeR (Ardón et al., 2013). Flooding during storm surges is another mechanism by which surface water can facilitate saltwater incursion (Klassen and Allen, 2017). Saltwater incursion via either mechanism, drought or storm surge, deposits SO_4^{2-} in the soil (Ardón et al., 2013; Schoepfer et al., 2014). This SO_4^{2-} influx could persist in the soil and be internally transformed to other S species (sulfite, thiosulfate, sulfide, S^0) (Ghosh and Dam, 2009; Rückert, 2016; Schoepfer et al., 2014).

Because the S from saltwater can persist in the soil, changes in soil O_2 availability due to precipitation or dry down are important for structuring anaerobic and aerobic S metabolisms following the saltwater incursion event (Schoepfer et al., 2014). Assimilatory SO_4^{2-} reduction is a highly conserved process, used by both aerobic and anaerobic organisms (Rückert, 2016). On the other hand, anaerobic microorganisms participate in dissimilatory SO_4^{2-} reduction (Rückert, 2016). Both assimilatory and dissimilatory SO_4^{2-} reduction produce hydrogen sulfide (H_2S) (Rückert, 2016). In assimilatory SO_4^{2-} reduction, H_2S is produced as an intermediate that is incorporated into biomolecules (Rückert, 2016). In contrast, dissimilatory SO_4^{2-} reduction produces H_2S as a waste product, in larger quantities than assimilatory SO_4^{2-} reduction, and is therefore, a more important metabolism to consider during freshwater ecosystem sulfidization events (Hopfensperger et al., 2014; Rückert, 2016; Schoepfer et al., 2014).

While SO_4^{2-} reduction described above consumes SO_4^{2-}, thiosulfate oxidation by the SOX complex produces SO_4^{2-} (Ghosh and Dam, 2009; Rückert, 2016). Phototrophs, mixotrophs, and heterotrophs participate in thiosulfate oxidation via the SOX complex in a variety of assimilatory and dissimilatory and aerobic and anaerobic pathways (Ghosh and Dam, 2009). In the context of a microbial community, thiosulfate oxidation (and S oxidation pathways in general) is important for regenerating oxidized S species (i.e., SO_4^{2-}) that can again be reduced by sulfate-reducing microorganism (Ghosh and Dam, 2009). In the current study, hydrologic history influenced the composition of thiosulfate oxidation by SOX complex genes, but it is not clear which historical conditions (i.e., wet or dry) differentiated thiosulfate oxidation (Table S4).

A variety of electron acceptors can be used in the oxidation of thiosulfate (Ghosh and Dam, 2009). In freshwater wetlands in Michigan, NO_3^- reduction contributed to SO_4^{2-} production via oxidation of sulfide (Burgin and Hamilton, 2008). Of the two major NO_3^- reduction pathways, denitrification and DNRA, S-driven denitrification made up a greater fraction of NO_3^- removal, but S-driven DNRA also contributed significantly to NO_3^- removal (Burgin and Hamilton, 2008). To test for NO_3^--driven SO_4^{2-} production in our mesocosm experiment, we measured correlations between the Bray-Curtis distance matrices of denitrification genes and thiosulfate oxidation genes, and DNRA genes and thiosulfate oxidation genes. We found that DNRA was significantly correlated to thiosulfate oxidation by SOX complex ($R = 0.196$, $P = 0.0499$; Table S1), but denitrification was not correlated to thiosulfate oxidation by SOX complex ($R = 0.117$, $P = 0.170$; Table S1). It is difficult to predict the balance of denitrification and DNRA in a given system, but some evidence supports the importance of NO_3^- loading and the oxidation state of S sources (Jia et al., 2020; Koop-Jakobsen and Giblin, 2010; Li et al., 2022). Interestingly, Li and colleagues found thiosulfate oxidation to be strongly coupled with denitrification, but not at all coupled with

DNRA (2022). It is possible that in the thiosulfate enrichment incubation experiment performed by Li and colleagues (2022), denitrifying microorganisms outcompeted DNRA bacteria by rapidly consuming added thiosulfate (Li et al., 2022). It is unclear whether these results showed an inability of DNRA bacteria to use thiosulfate as an electron donor, or if denitrifiers simply outcompeted DNRA bacteria for thiosulfate (Li et al., 2022). Further work is required to understand the connections between DNRA and thiosulfate oxidation in TOWeR sediments.

Hydrologic History Influences Iron Functional Gene Composition

Hydrologic history modified Fe functional gene composition. Specifically, hydrologic history altered the composition all Fe genes identified by FeGenie and the subset of Fe reduction genes identified by FeGenie (Table S5). Transformations of Fe vary based on the environmental redox status and pH of the environment (Weber et al., 2006). It follows that dry or wet, and oxic or anoxic historical conditions would structure different Fe cycling communities. In anoxic environments (with pH > 4), microbial Fe(III) reduction is a major electron sink for organic matter oxidation (Canfield et al., 1993; Weber et al., 2006). Therefore, greater genetic potential for Fe reduction may exist in historically wet soils with presumably lower O_2 availability. But this inference is complicated by the ongoing microbial transformations of N alongside aerobic and anaerobic oxidations and reductions of Fe (reviewed in Weber et al., 2006). Our analysis of the composition of all Fe genes identified by FeGenie highlights the impact of hydrologic history on Fe cycling, and Fe reduction specifically.

FeGenie was developed in response to a lack of Fe annotation tools (Garber et al., 2020). Prior to FeGenie, one of the few options for identifying Fe reduction genes was TIGRFAMS mtrB (TIGR03509) and mtrC (TIGR03507) (Garber et al., 2020). We also used the composition of TIGR03509 and TIGR03507 to analyze Fe reduction composition and found the composition to

differ by plant (presence/absence) and hydrologic treatment (Table S5). TIGR03509 and TIGR03507 are included in FeGenie, but FeGenie and IMG's TIGRFAM annotation pipeline resulted in different counts of mtrB and mtrC. These different results from different annotation tools highlight the current uncertainties in Fe gene annotation and point towards a need for increased consensus in Fe gene annotation.

Sulfate Reduction and Iron Reduction Correlate in Reducing Conditions and Influence Greenhouse Gas Concentrations

We hypothesized that SO_4^{2-} reduction and Fe reduction would be coupled (meaning significantly correlated) in reducing (i.e., flooded) conditions. We found that the functional gene composition of SO_4^{2-} reduction and Fe reduction genes were significantly correlated in the wet treatment, but not in the wet history, or either of dry hydrologic treatment or history (Table S2). This indicates that the functional gene composition of both metabolisms responded similarly and strongly to eight weeks of flooding. Both SO_4^{2-} reduction and Fe reduction are metabolisms commonly found in anoxic sediments (Flynn et al., 2021). The wet treatment appears to have imposed suboxic/anoxic conditions, characterized by a higher percent of paint removed from IRIS tubes (Figure 3C), and these reducing conditions were likely conducive to both SRM and FeRM. This supports previous findings of correlated SO_4^{2-} and Fe reduction in TOWeR soils (Schoepfer et al., 2014).

In addition to the iron-sulfur linkages described above, SO_4^{2-} reduction and Fe reduction gene compositions showed linkages with production of CO_2 and CH_4. The functional gene composition of assimilatory SO_4^{2-} reduction correlated with measured CO_2 concentrations (Figure 5B). The CO_2 concentrations were greater in dry treatments than in wet treatments (Figure 4B).

This may indicate that CO_2 production linked to assimilatory SO_4^{2-} reduction was favored in dry, oxidizing conditions.

Dissimilatory SO_4^{2-} reduction gene composition and Fe reduction gene composition (Week 8 only) were both significantly correlated with CH_4 concentrations (Figure 6C, 8B). This compositional approach showed that variation in gene compositions corresponded with variations in CH_4 concentrations but does not reveal linear relationships between gene abundance and CH_4 concentration. Therefore, relationships between SO_4^{2-}/Fe reduction genes and CH_4 could be positive (increased gene abundance with increased CH_4 concentrations) or negative (increased gene abundance with decreased CH_4 concentrations, or vice-versa). Explanations for both positive and negative relationships between SO_4^{2-}/Fe reduction genes and CH_4 concentrations are possible. Dissimilatory SO_4^{2-} reduction, Fe reduction, and methanogenesis are all generally considered anaerobic metabolisms (Flynn et al., 2021; Lyu et al., 2018). Therefore, the reducing or oxidizing environment (e.g., wet vs. dry conditions) could have impacted all three metabolisms similarly, resulting in the observed correlations. Alternatively, the correlations between dissimilatory SO_4^{2-} reduction and CH_4 concentrations, and Fe reduction and CH_4 concentrations, could be the result of competition between microbial taxa. Since Fe reduction and dissimilatory SO_4^{2-} reduction are more thermodynamically favorable than methanogenesis (in standard conditions) (Wang et al., 2017), it is conceivable that when FeRM and SRM are abundant (because Fe(III) and SO_4^{2-} are available), these microbial communities outcompete the less abundant methanogens, resulting in a negative correlation. Similarly, methanogenic archaea may switch from methanogenesis to Fe reduction when resources allow (Sivan et al., 2016). But importantly, soil microbial communities do not exist in standard conditions, and thermodynamics are insufficient to explain community metabolic interactions (Bethke et al., 2011). In addition, soil pH may be more important for

structuring soil microbial communities than the thermodynamic favorability of metabolic processes. A known mutualism between SRM and methanogens exists, in which methanogens consume H_2S produced by SRM, and thereby maintain the required pH for both SO_4^{2-} reduction and methanogenesis to proceed (Bethke et al., 2011; Fierer and Jackson, 2006; Shi et al., 2020).

CONCLUSION

An oversimplified view of biogeochemistry might describe the biogeochemical cycles of C, N, Fe, and S in isolation, with transformations structured in communities according to thermodynamic favorability (Bethke et al., 2011; Schlesinger et al., 2011). But it is increasingly clear that biogeochemical cycles are intertwined, and a "microbial energy economy" that relies on resource availability and biotic/abiotic interactions is closer to reality than a hierarchically structured thermodynamic ladder (Bethke et al., 2011; Burgin et al., 2011). The specific biotic and abiotic context in which communities are found will likely determine which linkages between cycles are relevant. In the TOWeR soil mesocosms in this study, Fe-rich soils and seasonal saltwater intrusion importing SO_4^{2-} make Fe and S linkages with C and N metabolism particularly relevant. Considering linked biogeochemical and the historical context of an ecosystem will help improve predictions of the future impacts of sea-level rise on coastal biogeochemistry.

REFERENCES

Ardón, M., Morse, J.L., Colman, B.P., Bernhardt, E.S., 2013. Drought-induced saltwater incursion leads to increased wetland nitrogen export. Global Change Biology 19, 2976–2985. https://doi.org/10.1111/gcb.12287

Bethke, C.M., Sanford, R.A., Kirk, M.F., Jin, Q., Flynn, T.M., 2011. The thermodynamic ladder in geomicrobiology. American Journal of Science 311, 183–210. https://doi.org/10.2475/03.2011.01

Bledsoe, R.B., Finlay, C.G., Peralta, A.L., 2023. Plant-microbe-mediated decrease of greenhouse gases under dynamic wetland hydrology. https://doi.org/10.1101/2020.06.29.178533

Bowers, R.M., Kyrpides, N.C., Stepanauskas, R., Harmon-Smith, M., Doud, D., Reddy, T.B.K., Schulz, F., Jarett, J., Rivers, A.R., Eloe-Fadrosh, E.A., Tringe, S.G., Ivanova, N.N., Copeland, A., Clum, A., Becraft, E.D., Malmstrom, R.R., Birren, B., Podar, M., Bork, P., Weinstock, G.M., Garrity, G.M., Dodsworth, J.A., Yooseph, S., Sutton, G., Glöckner, F.O., Gilbert, J.A., Nelson, W.C., Hallam, S.J., Jungbluth, S.P., Ettema, T.J.G., Tighe, S., Konstantinidis, K.T., Liu, W.-T., Baker, B.J., Rattei, T., Eisen, J.A., Hedlund, B., McMahon, K.D., Fierer, N., Knight, R., Finn, R., Cochrane, G., Karsch-Mizrachi, I., Tyson, G.W., Rinke, C., Lapidus, A., Meyer, F., Yilmaz, P., Parks, D.H., Murat Eren, A., Schriml, L., Banfield, J.F., Hugenholtz, P., Woyke, T., 2017. Minimum information about a single amplified genome (MISAG) and a metagenome-assembled genome (MIMAG) of bacteria and archaea. Nat Biotechnol 35, 725–731. https://doi.org/10.1038/nbt.3893

Burgin, A.J., Hamilton, S.K., 2008. NO3−-Driven SO42− Production in Freshwater Ecosystems: Implications for N and S Cycling. Ecosystems 11, 908–922. https://doi.org/10.1007/s10021-008-9169-5

Burgin, A.J., Yang, W.H., Hamilton, S.K., Silver, W.L., 2011. Beyond carbon and nitrogen: how the microbial energy economy couples elemental cycles in diverse ecosystems. Frontiers in Ecology and the Environment 9, 44–52. https://doi.org/10.1890/090227

Canfield, D.E., Jørgensen, B.B., Fossing, H., Glud, R., Gundersen, J., Ramsing, N.B., Thamdrup, B., Hansen, J.W., Nielsen, L.P., Hall, P.O.J., 1993. Pathways of organic carbon oxidation in three continental margin sediments. Marine Geology, Marine Sediments, Burial, Pore Water Chemistry, Microbiology and Diagenesis 113, 27–40. https://doi.org/10.1016/0025-3227(93)90147-N

Chen, I.-M.A., Markowitz, V.M., Chu, K., Palaniappan, K., Szeto, E., Pillay, M., Ratner, A., Huang, J., Andersen, E., Huntemann, M., Varghese, N., Hadjithomas, M., Tennessen, K., Nielsen, T., Ivanova, N.N., Kyrpides, N.C., 2017. IMG/M: integrated genome and metagenome comparative data analysis system. Nucleic Acids Research 45, D507–D516. https://doi.org/10.1093/nar/gkw929

Chilton, D., Hamilton, D.P., Nagelkerken, I., Cook, P., Hipsey, M.R., Reid, R., Sheaves, M., Waltham, N.J., Brookes, J., 2021. Environmental Flow Requirements of Estuaries: Providing Resilience to Current and Future Climate and Direct Anthropogenic Changes. Frontiers in Environmental Science 9.

Colmer, T.D., 2003. Long-distance transport of gases in plants: a perspective on internal aeration and radial oxygen loss from roots. Plant, Cell & Environment 26, 17–36. https://doi.org/10.1046/j.1365-3040.2003.00846.x

Conley, D.J., Paerl, H.W., Howarth, R.W., Boesch, D.F., Seitzinger, S.P., Havens, K.E., Lancelot, C., Likens, G.E., 2009. Controlling Eutrophication: Nitrogen and Phosphorus. Science 323, 1014–1015. https://doi.org/10.1126/science.1167755

Cook, F.J., Knight, J.H., 2003. Oxygen Transport to Plant Roots. Soil Science Society of America Journal 67, 20–31. https://doi.org/10.2136/sssaj2003.2000

Crowther, T.W., van den Hoogen, J., Wan, J., Mayes, M.A., Keiser, A.D., Mo, L., Averill, C., Maynard, D.S., 2019. The global soil community and its influence on biogeochemistry. Science 365, eaav0550. https://doi.org/10.1126/science.aav0550

DeAngelis, K.M., Silver, W.L., Thompson, A.W., Firestone, M.K., 2010. Microbial communities acclimate to recurring changes in soil redox potential status. Environmental Microbiology 12, 3137–3149. https://doi.org/10.1111/j.1462-2920.2010.02286.x

Dlamini, J.C., Chadwick, D., Hawkins, J.M.B., Martinez, J., Scholefield, D., Ma, Y., Cárdenas, L.M., 2020. Evaluating the potential of different carbon sources to promote denitrification. The Journal of Agricultural Science 158, 194–205. https://doi.org/10.1017/S0021859620000520

Esposti, M.D., 2020. On the evolution of cytochrome oxidases consuming oxygen. Biochimica et Biophysica Acta (BBA) - Bioenergetics 1861, 148304. https://doi.org/10.1016/j.bbabio.2020.148304

Falkowski, P.G., Fenchel, T., Delong, E.F., 2008. The Microbial Engines That Drive Earth's Biogeochemical Cycles. Science 320, 1034–1039. https://doi.org/10.1126/science.1153213

Fierer, N., Jackson, R.B., 2006. The diversity and biogeography of soil bacterial communities. Proceedings of the National Academy of Sciences 103, 626–631. https://doi.org/10.1073/pnas.0507535103

Flynn, T.M., Antonopoulos, D.A., Skinner, K.A., Brulc, J.M., Johnston, E., Boyanov, M.I., Kwon, M.J., Kemner, K.M., O'Loughlin, E.J., 2021. Biogeochemical dynamics and microbial community development under sulfate- and iron-reducing conditions based on electron shuttle amendment. PLOS ONE 16, e0251883. https://doi.org/10.1371/journal.pone.0251883

Garber, A.I., Nealson, K.H., Okamoto, A., McAllister, S.M., Chan, C.S., Barco, R.A., Merino, N., 2020. FeGenie: A Comprehensive Tool for the Identification of Iron Genes and Iron Gene Neighborhoods in Genome and Metagenome Assemblies. Frontiers in Microbiology 11.

Ghosh, W., Dam, B., 2009. Biochemistry and molecular biology of lithotrophic sulfur oxidation by taxonomically and ecologically diverse bacteria and archaea. FEMS Microbiology Reviews 33, 999–1043. https://doi.org/10.1111/j.1574-6976.2009.00187.x

Glass, J.B., Elbon, C.E., Williams, L.D., 2022. Something old, something new, something borrowed, something blue: the anaerobic microbial ancestry of aerobic respiration. Trends in Microbiology 0. https://doi.org/10.1016/j.tim.2022.08.006

Herbert, E.R., Boon, P., Burgin, A.J., Neubauer, S.C., Franklin, R.B., Ardón, M., Hopfensperger, K.N., Lamers, L.P.M., Gell, P., 2015. A global perspective on wetland salinization: ecological consequences of a growing threat to freshwater wetlands. Ecosphere 6, art206. https://doi.org/10.1890/ES14-00534.1

Herbert, E.R., Schubauer-Berigan, J., Craft, C.B., 2018. Differential effects of chronic and acute simulated seawater intrusion on tidal freshwater marsh carbon cycling. Biogeochemistry 138, 137–154. https://doi.org/10.1007/s10533-018-0436-z

Hopfensperger, K.N., Burgin, A.J., Schoepfer, V.A., Helton, A.M., 2014. Impacts of Saltwater Incursion on Plant Communities, Anaerobic Microbial Metabolism, and Resulting Relationships in a Restored Freshwater Wetland. Ecosystems 17, 792–807. https://doi.org/10.1007/s10021-014-9760-x

Jabłońska, J., Tawfik, D.S., 2019. The number and type of oxygen-utilizing enzymes indicates aerobic vs. anaerobic phenotype. Free Radic Biol Med 140, 84–92. https://doi.org/10.1016/j.freeradbiomed.2019.03.031

Jenkinson, B.J., Franzmeier, D.P., 2006. Development and Evaluation of Iron-Coated Tubes that Indicate Reduction in Soils. Soil Science Society of America Journal 70, 183–191. https://doi.org/10.2136/sssaj2004.0323

Jia, M., Winkler, M.K.H., Volcke, E.I.P., 2020. Elucidating the Competition between Heterotrophic Denitrification and DNRA Using the Resource-Ratio Theory. Environ. Sci. Technol. 54, 13953–13962. https://doi.org/10.1021/acs.est.0c01776

Johnston, E.R., Hatt, J.K., He, Z., Wu, L., Guo, X., Luo, Y., Schuur, E.A.G., Tiedje, J.M., Zhou, J., Konstantinidis, K.T., 2019. Responses of tundra soil microbial communities to half a decade of experimental warming at two critical depths. Proceedings of the National Academy of Sciences 116, 15096–15105. https://doi.org/10.1073/pnas.1901307116

Klassen, J., Allen, D.M., 2017. Assessing the risk of saltwater intrusion in coastal aquifers. Journal of Hydrology, Investigation of Coastal Aquifers 551, 730–745. https://doi.org/10.1016/j.jhydrol.2017.02.044

Koop-Jakobsen, K., Giblin, A.E., 2010. The effect of increased nitrate loading on nitrate reduction via denitrification and DNRA in salt marsh sediments. Limnology and Oceanography 55, 789–802. https://doi.org/10.4319/lo.2010.55.2.0789

Koop-Jakobsen, K., Wenzhöfer, F., 2015. The Dynamics of Plant-Mediated Sediment Oxygenation in Spartina anglica Rhizospheres—a Planar Optode Study. Estuaries and Coasts 38, 951–963. https://doi.org/10.1007/s12237-014-9861-y

Kozlowski, T.T., 1984. Plant Responses to Flooding of Soil. BioScience 34, 162–167. https://doi.org/10.2307/1309751

Kuypers, M.M.M., Marchant, H.K., Kartal, B., 2018. The microbial nitrogen-cycling network. Nat Rev Microbiol 16, 263–276. https://doi.org/10.1038/nrmicro.2018.9

Lamers, L.P.M., Govers, L.L., Janssen, I.C.J.M., Geurts, J.J.M., Van der Welle, M.E.W., Van Katwijk, M.M., Van der Heide, T., Roelofs, J.G.M., Smolders, A.J.P., 2013. Sulfide as a soil phytotoxin—a review. Front Plant Sci 4, 268. https://doi.org/10.3389/fpls.2013.00268

Li, S., Jiang, Z., Ji, G., 2022. Effect of sulfur sources on the competition between denitrification and DNRA. Environmental Pollution 305, 119322. https://doi.org/10.1016/j.envpol.2022.119322

Liu, Y.-R., Delgado-Baquerizo, M., Yang, Z., Feng, J., Zhu, J., Huang, Q., 2020. Microbial taxonomic and functional attributes consistently predict soil CO2 emissions across contrasting croplands. Science of The Total Environment 702, 134885. https://doi.org/10.1016/j.scitotenv.2019.134885

Lyu, Z., Shao, N., Akinyemi, T., Whitman, W.B., 2018. Methanogenesis. Current Biology 28, R727–R732. https://doi.org/10.1016/j.cub.2018.05.021

Mehlich, A., 1984. Mehlich 3 soil test extractant: A modification of Mehlich 2 extractant. Communications in Soil Science and Plant Analysis 15, 1409–1416. https://doi.org/10.1080/00103628409367568

Oksanen, J., Simpson, G., Blanchet, F., Kindt, R., Legendre, P., Minchin, P., O'Hara, R., Solymos, P., Stevens, M., Szoecs, E., Wagner, H., Barbour, M., Bedward, M., Bolker, B., Borcard, D., Carvalho, G., Chirico, M., De Caceres, M., Durand, S., Evangelista, H., FitzJohn, R., Friendly, M., Furneaux, B., Hannigan, G., Hill, M., Lahti, L., McGlinn, D., Ouellette, M., Ribeiro Cunha, Smith, T., Stier, A., Ter Braak, C., Weedon, J., 2022. vegan: Community Ecology Package.

Patrick Jr., W.H., Jugsujinda, A., 1992. Sequential Reduction and Oxidation of Inorganic Nitrogen, Manganese, and Iron in Flooded Soil. Soil Science Society of America Journal 56, 1071–1073. https://doi.org/10.2136/sssaj1992.03615995005600040011x

Peralta, A.L., Bledsoe, R.B., Muscarella, M.E., Huntemann, M., Clum, A., Foster, Brian, Foster, Bryce, Roux, S., Palaniappan, K., Varghese, N., Mukherjee, S., Reddy, T.B.K., Daum, C., Copeland, A., Chen, I.-M.A., Ivanova, N.N., Kyrpides, N.C., Glavina del Rio, T., Eloe-Fadrosh, E.A., 2020. Metagenomes from Experimental Hydrologic Manipulation of Restored Coastal Plain Wetland Soils (Tyrell County, North Carolina). Microbiol Resour Announc 9. https://doi.org/10.1128/MRA.00882-20

Peralta, A.L., Ludmer, S., Kent, A.D., 2013. Hydrologic history influences microbial community composition and nitrogen cycling under experimental drying/wetting treatments. Soil Biology and Biochemistry 66, 29–37. https://doi.org/10.1016/j.soilbio.2013.06.019

Peralta, A.L., Ludmer, S., Matthews, J.W., Kent, A.D., 2014. Bacterial community response to changes in soil redox potential along a moisture gradient in restored wetlands. Ecological Engineering 73, 246–253. https://doi.org/10.1016/j.ecoleng.2014.09.047

Pezeshki, S.R., DeLaune, R.D., 2012. Soil Oxidation-Reduction in Wetlands and Its Impact on Plant Functioning. Biology 1, 196–221. https://doi.org/10.3390/biology1020196

Pörtner, H.-O., Roberts, D.C., Adams, H., Adelekan, I., Adler, I., Adrian, C., Aldunce, P., Bowen, K., Caretta, M.A., Carnicer, J., Castellanos, E., Cheong, T.S., Chow, W., Cissé, G., Zaiton, Z., 2022. CLIMATE CHANGE 2022 IMPACTS, ADAPTATION AND VULNERABILITY, 1ST ED. ed, Technical Summary. CAMBRIDGE UNIV PRESS UK, Cambridge, UK and New York, USA.

Quince, C., Walker, A.W., Simpson, J.T., Loman, N.J., Segata, N., 2017. Shotgun metagenomics, from sampling to analysis. Nat Biotechnol 35, 833–844. https://doi.org/10.1038/nbt.3935

R Core Team, 2023. R: A Language and Environment for Statistical Computing.

Rabenhorst, M.C., 2008. Protocol for Using and Interpreting IRIS Tubes. Soil Survey Horizons 49, 74–77.

RoyChowdhury, T., Bramer, L., Hoyt, D.W., Kim, Y.-M., Metz, T.O., McCue, L.A., Diefenderfer, H.L., Jansson, J.K., Bailey, V., 2018. Temporal dynamics of CO2 and CH4 loss potentials in response to rapid hydrological shifts in tidal freshwater wetland soils. Ecological Engineering, Wetlands and Carbon Revisited 114, 104–114. https://doi.org/10.1016/j.ecoleng.2017.06.041

Rückert, C., 2016. Sulfate reduction in microorganisms—recent advances and biotechnological applications. Current Opinion in Microbiology, Antimicrobials • Microbial systems biology 33, 140–146. https://doi.org/10.1016/j.mib.2016.07.007

Schlesinger, W.H., Cole, J.J., Finzi, A.C., Holland, E.A., 2011. Introduction to coupled biogeochemical cycles. Frontiers in Ecology and the Environment 9, 5–8. https://doi.org/10.1890/090235

Schneider, C.A., Rasband, W.S., Eliceiri, K.W., 2012. NIH Image to ImageJ: 25 years of image analysis. Nature Methods 9, 671–675. https://doi.org/10.1038/nmeth.2089

Schoepfer, V.A., Bernhardt, E.S., Burgin, A.J., 2014. Iron clad wetlands: Soil iron-sulfur buffering determines coastal wetland response to salt water incursion. Journal of Geophysical Research: Biogeosciences 119, 2209–2219. https://doi.org/10.1002/2014JG002739

Shi, X., Gao, G., Tian, J., Wang, X.C., Jin, X., Jin, P., 2020. Symbiosis of sulfate-reducing bacteria and methanogenic archaea in sewer systems. Environment International 143, 105923. https://doi.org/10.1016/j.envint.2020.105923

Sivan, O., Shusta, S.S., Valentine, D.L., 2016. Methanogens rapidly transition from methane production to iron reduction. Geobiology 14, 190–203. https://doi.org/10.1111/gbi.12172

Tiedje, J.M., Simkins, S., Groffman, P.M., 1989. Perspectives on measurement of denitrification in the field including recommended protocols for acetylene based methods. Plant Soil 115, 261–284. https://doi.org/10.1007/BF02202594

Toole, D.R., Zhao, J., Martens-Habbena, W., Strauss, S.L., 2021. Bacterial functional prediction tools detect but underestimate metabolic diversity compared to shotgun metagenomics in

southwest Florida soils. Applied Soil Ecology 168, 104129. https://doi.org/10.1016/j.apsoil.2021.104129

Wallenstein, M.D., Myrold, D.D., Firestone, M., Voytek, M., 2006. Environmental Controls on Denitrifying Communities and Denitrification Rates: Insights from Molecular Methods. Ecological Applications 16, 2143–2152. https://doi.org/10.1890/1051-0761(2006)016[2143:ECODCA]2.0.CO;2

Wang, Q., Alowaifeer, A., Kerner, P., Balasubramanian, N., Patterson, A., Christian, W., Tarver, A., Dore, J.E., Hatzenpichler, R., Bothner, B., McDermott, T.R., 2021. Aerobic bacterial methane synthesis. PNAS 118. https://doi.org/10.1073/pnas.2019229118

Wang, X.-N., Sun, G.-X., Zhu, Y.-G., 2017. Thermodynamic energy of anaerobic microbial redox reactions couples elemental biogeochemical cycles. J Soils Sediments 17, 2831–2846. https://doi.org/10.1007/s11368-017-1767-4

Weber, K.A., Achenbach, L.A., Coates, J.D., 2006. Microorganisms pumping iron: anaerobic microbial iron oxidation and reduction. Nat Rev Microbiol 4, 752–764. https://doi.org/10.1038/nrmicro1490

APPENDIX: SUPPLEMENTAL RESULTS AND DISCUSSION

Supplemental Results (presented in Bledsoe et al., 2023)

Greenhouse Gas Concentrations

Within no-plant treatments, wet (19.9 ± 42.0 mg CH_4-C m^{-2}, average ± SD) and interim (6.5 ± 25.4 mg CH_4-C m^{-2}) hydrologic treatments produced the highest CH_4 concentrations and the greatest variability between samples compared to dry treatments (0.22 ± 0.93) (Figure 4A). Within no-plant treatments, dry (104.7 ± 37.4 mg CO_2-C m^{-2}), interim (58.1 ± 30.6 mg CO_2-C m^{-2}), and wet (42.3 ± 18.5 mg CO_2-C m^{-2}) hydrologic treatments produced the highest CO_2 concentrations compared to treatments with plants (35.1 ± 19.2, 29.5 ± 15.0, 24.9 ± 0.6 mg CO_2-C m^{-2}, respectively) (Figure 4B). The N_2O concentrations were near zero in all hydrologic and plant treatments (range: 0.05-0.15 mg N_2O-N m^{-2}) (Figure 4C).

Functional Genes

The four functional gene categories (denitrification, methanogenesis, central carbohydrate metabolism, and cytochrome C oxidase (CcO)) showed varying responses to plant and hydrologic treatment but no response to interactions between plant and hydrologic treatments. Carbohydrate metabolic composition differed between hydrologic treatment (PERMANOVA, $F_{1, 23} = 2.735$, $R^2 = 0.092$, $P = 0.012$; Table S5), but was similar across plant presence and absence (PERMANOVA, $F_{2, 23} = 0.998$, $R^2 = 0.067$, $P = 0.423$; Table S5). In contrast, the compositions of denitrification genes (PERMANOVA, plant: $F_{2, 23} = 0.840$, $R^2 = 0.086$, $P = 0.576$, treatment: $F_{1, 23} = 0.667$, $R^2 = 0.034$, $P = 0.622$; Table S5), methanogenesis genes (PERMANOVA, plant: $F_{2, 23} = 1.045$, $R^2 = 0.085$, $P = 0.406$, treatment: $F_{1, 23} = 1.184$, $R^2 = 0.048$, $P = 0.314$), and CcO genes (PERMANOVA, plant: $F_{2, 23} = 1.211$, $R^2 = 0.076$, $P = 0.316$, treatment: $F_{1, 23} = 0.977$, $R^2 = 0.031$, $P = 0.418$; Table

S5) were similar across plant presence and hydrologic treatments. Plant presence/absence had no significant impact on the composition of functional genes.

Microbial Structure-Function Relationships

Based on environmental fitting (vegan::envfit), functional gene composition correlated to carbon losses (CO_2 and CH_4 production) (Figure S1). Specifically, CO_2 concentrations correlated to the PCoA ordinations of both denitrification (envfit, $R^2 = 0.25$, $P = 0.05$) and carbohydrate metabolism (envfit, $R^2 = 0.23$, $P = 0.06$), while the ordination of the methanogenesis genes had a marginally good fit with CH_4 production (envfit, $R^2 = 0.20$, $P = 0.09$) (Figure S1). We also evaluated relationships among variation in GHG concentrations and variation in functional gene composition at the beginning ('Week 0') and end of the experiment ('Week 8') using distance-based partial least square regression. Denitrification gene composition explained 31.56% of variation in N_2O production at the start of the experiment, and 74.50% of variation in N_2O production at the end of the experiment. Methanogenesis functional gene variation explained a higher proportion of CH_4 production in 'Week 0' samples (49.87%) than 'Week 8' samples (17.65%). 'Week 0' compositions of carbohydrate metabolism, CcO, and denitrification genes, respectively, explained 72.26%, 40.85%, and 32.47% of variation in CO_2. By the end of the experiment, CcO composition could only account for 6.78% of CO_2 production, while carbohydrate metabolism and denitrification explained 40.12% and 50.75% of the variation in CO_2 production, respectively.

Supplemental Discussion (presented in Bledsoe et al., 2023)

Mismatch Between Bacterial Community Composition and Greenhouse Gas Function

The DNA-based functional gene composition explained variation in GHG concentrations measured at the beginning of the experiment more than at the end of the experiment. Hydrologic

history influenced wetland soil microbial community composition more than contemporary treatments, which was emphasized in these results. The decrease in the strength of structure-function associations could be due to the DNA-based molecular measurement giving insight to historical and integrated environmental conditions and not contemporary changes to redox conditions. Another explanation of decreased structure-function associations could be due to the differences in temporal resolution measured by DNA-based molecular methods compared to the *in situ* greenhouse gas measurements.

Cytochrome C Oxidase

To further examine microbial functional composition and measured GHGs, we evaluated the composition of prokaryotic CcO genes as an indicator of aerobic respiration in more oxidizing redox conditions. While hydrologic history significantly influenced CcO composition (PERMANOVA, $F_{1, 23} = 7.224$, $R^2=0.227$, $P=0.001$, Table S5), CcO composition was unable to explain significant variations in GHG concentrations during the 8-week incubation (Figure S1). This lack of explanatory power is unsurprising, given the diversity of O_2-reducing terminal oxidases, and the known presence of CcO genes in strict anaerobes (Esposti, 2020; Jabłońska and Tawfik, 2019). There is no single enzyme that can be used to distinguish between aerobic and anaerobic phenotypes because aerobic and anaerobic organisms do not exist as binary groups (Jabłońska and Tawfik, 2019). Instead, a spectrum of O_2 usage phenotypes exists (Jabłońska and Tawfik, 2019). Evaluating the presence and number of a full suite of O_2-utilizing enzymes may be a useful indicator of aerobic vs. anaerobic status (Jabłońska and Tawfik, 2019). Therefore, bioinformatic methods to facilitate this method ought to be further developed.

Central Carbohydrate Metabolism

While CcO composition was unable to explain differences in CO_2 production across treatments, the composition of central carbohydrate metabolism genes was strongly related to differences in hydrologic history, hydrologic treatment, and the production of CO_2 (Figure S1, Tables S3 and S5). In a past study, results revealed a significant positive correlation between carbohydrate-active enzyme abundance and cumulative respiration in a tundra soil warming experiment (Johnston et al., 2019). Similarly, carbohydrate metabolism genes predicted differences in soil respiration between paddy and upland soils (Liu et al., 2020). While Johnston et al. also found a relationship between CcO relative abundance and reducing conditions, this was the only study we found that successfully used CcO genes as an indicator of redox conditions. Johnston et al. also found the total relative abundance of carbohydrate active enzyme genes was significantly positively related to cumulative ecosystem respiration (2019). Liu et al. found several carbohydrate metabolism genes to be significant predictors of respiration rates in upland versus paddy soils (2020). While there is no single gene or defined collection of genes that have been consistently used to explain microbial community respiration responses to redox changes, various collections of carbohydrate metabolism genes may reflect differences in soil redox status and respiration (Johnston et al., 2019; Liu et al., 2020).

Denitrification

When examining denitrifier community composition and greenhouse gas production, results showed that the composition of denitrification functional genes correlated to CO_2 concentrations but not N_2O concentrations (Figure S1). The lack of association with N_2O is unsurprising since denitrifier community composition included the suite of genes involved in the reduction of nitrate to dinitrogen gas. The association between denitrification and CO_2 production is likely the result of organic denitrification, where organic matter is oxidized to CO_2 with nitrate

as an electron acceptor (Dlamini et al., 2020; Schlesinger et al., 2011). Organic denitrification, a form of respiratory denitrification, is typically a facultative process, found in organisms with the ability to respire aerobically when oxygen is available, and use NO_3^- to respire anaerobically when oxygen availability decreases (Tiedje et al., 1989). A community-level denitrification response to soil hydrologic history and experimental drying/wetting has also been observed in a previous incubation experiment (Peralta et al., 2013).

Methanogenesis

In the present study, we observed that hydrologic history (more than contemporary hydrologic treatment) influenced methanogenesis functional gene composition (Figures 4 and S1, Table S5). Methanogenesis has historically been described as a specialized metabolism, in which methanogens are obligate anaerobes and obligate methanogens (meaning they do not use fermentation or alternative electron acceptors to grow) (Lyu et al., 2018). While atypical methanogenic pathways have recently been discovered (e.g., aerobic bacterial methane synthesis) (Wang et al., 2021), classical anaerobic methanogenesis is still recognized as the primary source of biogenic methane production (Lyu et al., 2018). In the present study, our results showed a strong influence of hydrologic history on methanogen functional gene composition, which supports the classical view of methanogenesis: a specialized and strictly anaerobic metabolism was maintained in the historically wet (i.e., low O_2) field conditions, and this history dictated mesocosms' methane production capacity. The structure-function analysis (based on DBPLSR) provides another line of evidence that hydrologic history influenced methane production, where methanogen functional gene composition explained a greater proportion of variation in CH_4 production at the start of the experiment, than at the end of the experiment (Table S3).

FIGURES AND TABLES

Figure 1

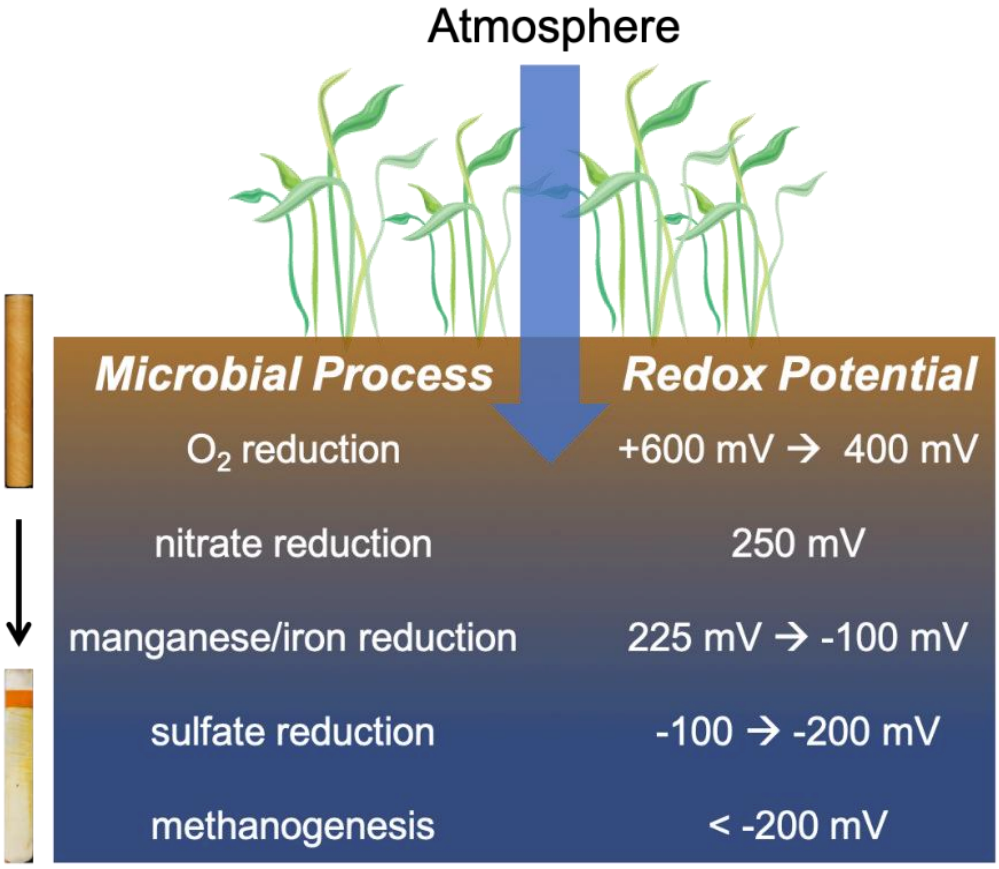

Figure 1. Conceptual diagram depicting relative ranges of redox potentials associated with predicted microbial processes. On the left side of the diagram, indicator for reduction in soils (IRIS) tubes are used to measure soil redox status, where iron oxide paint in orange represents oxidized (Fe(III)) conditions, and white represents reduced (Fe(II)) conditions.

Figure 2

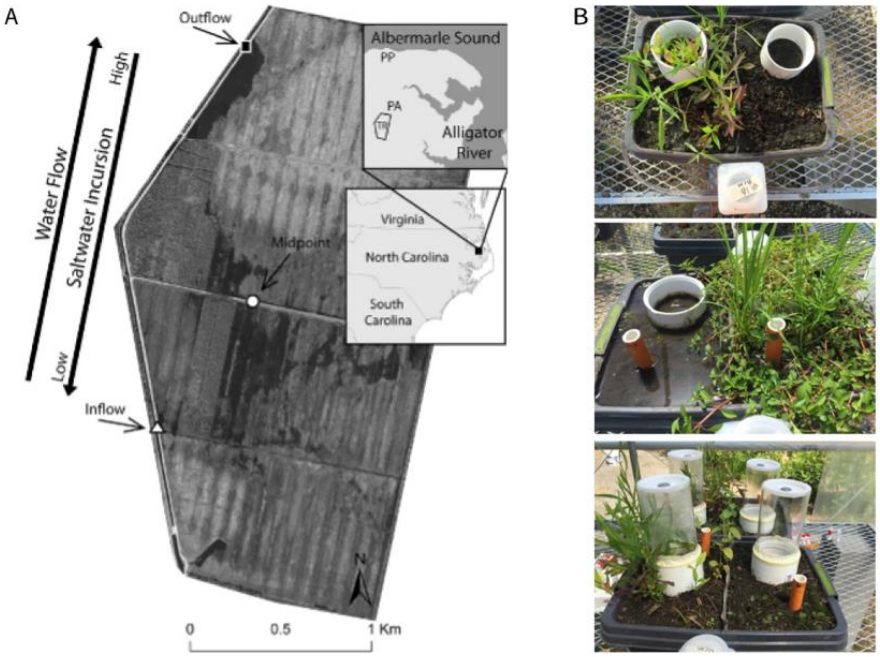

Figure 2. Field site sampling and experimental design of wetland mesocosm. Wetland mesocosms sourced from the Timberlake Observatory for Wetland Restoration field site (image modified from Ardón et al., 2013) (A). Aerial view of wetland mesocosm experiment, where the left side of box represents plant treatment, and the right side represents the no plant treatment separated by a stainless mesh divider (B, top panel). The PVC collars were installed for measuring greenhouse gas concentrations, and a 1-liter bottle attached to each side of the mesocosm was used to maintain water levels (B, top panel). Example of a wet treatment mesocosm with IRIS tubes installed (B, middle panel). Example of mesocosm with chambers prepared for GHG sampling (B, bottom panel).

Figure 3

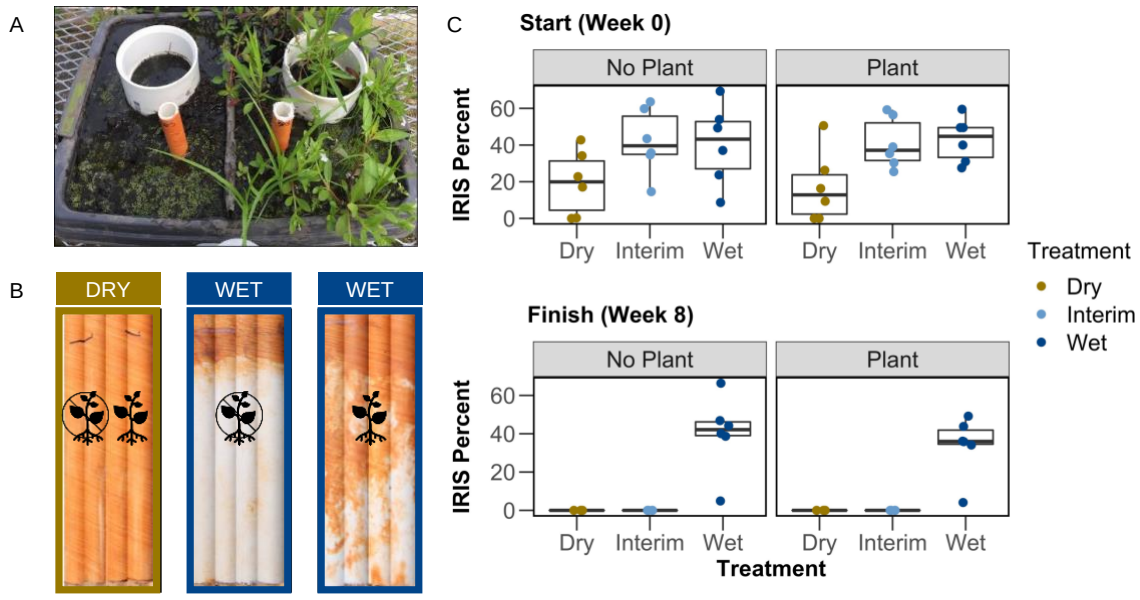

Figure 3. Measuring redox status in wetland mesocosms. Wetland mesocosm example showing indicator of reduction in soils (IRIS) tubes and PVC collar used for greenhouse gas measurements (A). Example IRIS tubes used for ImageJ analysis post-incubation associated with hydrologic treatment (top label) and plant treatment, where plant icons represent plant treatment and crossed out plant symbol represents no plant treatment (B). Boxplots summarize percent paint removed from IRIS tubes at start (week 0) and finish (week 8) of experimental incubation (C). Individual samples are plotted as filled circles, and symbol color represents hydrologic treatment (C). The boxplot is a visual representation of five key summary statistics: the median, the 25% and 75% percentiles, and the whiskers which represent the feasible range of the data as determined by 1.5 × the interquartile range. Symbols represent individual raw data points from four replicate samples.

Figure 4

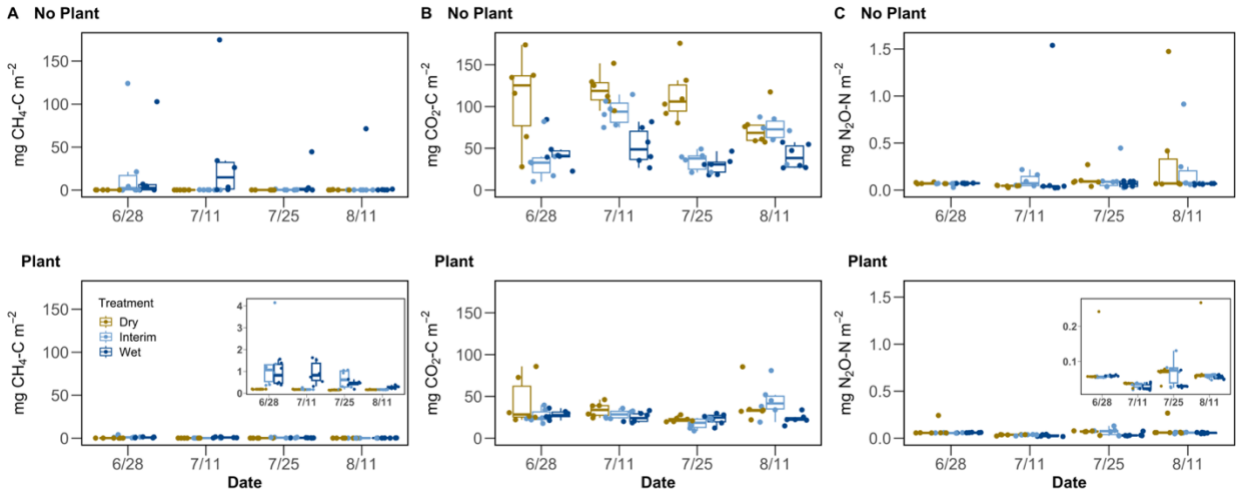

Figure 4. Boxplots of greenhouse gas concentrations. Methane (CH_4) (A), carbon dioxide (CO_2) (B), and nitrous oxide (N_2O) (C) concentrations by hydrologic treatment (Treatment), are shown during four timepoints (Date). Samples from No Plant mesocosms are shown in the top panel, while samples from mesocosms with plants are shown in the bottom panel. The insets in the bottom panels of (A) and (C) represent zoomed in y-axis scale of the same data. The boxplot is a visual representation of five key summary statistics: the median, the 25% and 75% percentiles, and the whiskers which represent the feasible range of the data as determined by 1.5 × the interquartile range. Symbols represent individual raw data points from four replicate samples.

Figure 5

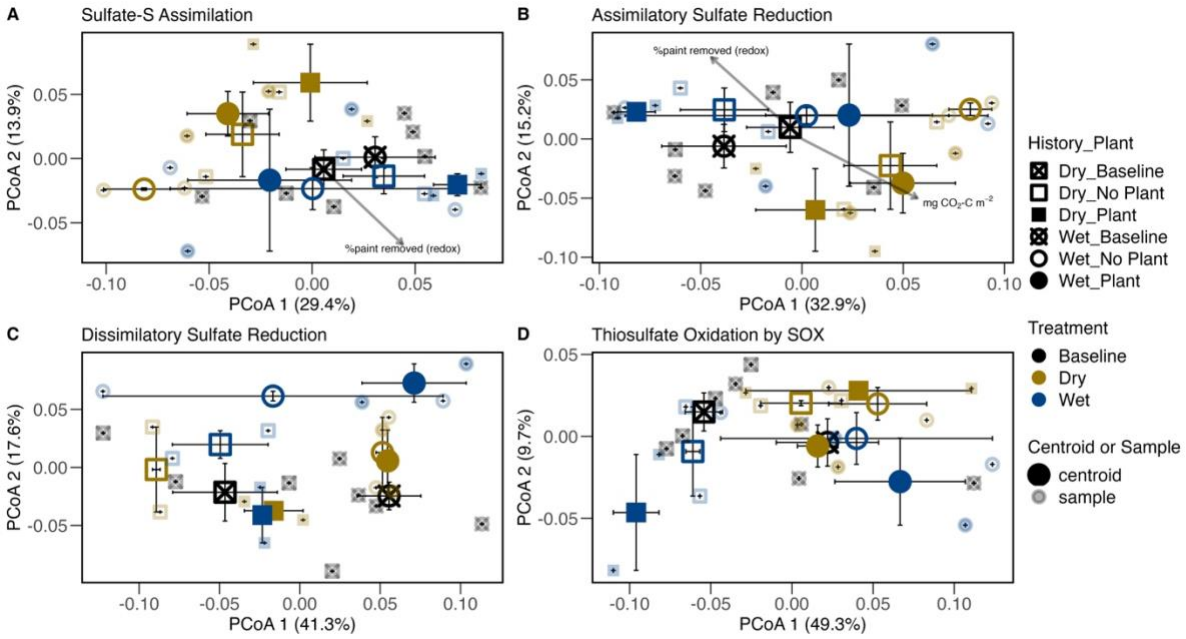

Figure 5. Ordination of sulfur functional gene modules. Ordinations are based on principal coordinates analysis (PCoA), depicting community composition of the sulfur functional gene modules Sulfate-Sulfur Assimilation (M00616) (A), Assimilatory Sulfate Reduction (M00176) (B), Dissimilatory Sulfate Reduction (M00596) (C), and Thiosulfate Oxidation by SOX Complex (M00595) (D). Percent variation explained by each axis is listed in parentheses. Colors refer to hydrologic treatments, where black = baseline, brown = dry, dark blue = wet. Shapes refer to hydrologic history of the sample, where square = dry, circle = wet. The shape fill represents plant treatment, where 'x' through symbol = baseline, open symbol = no plant, closed symbol = plant. Baseline samples were collected before the start of hydrologic and plant treatments and treatment samples were collected after eight weeks. Vectors represent significant ($P < 0.05$) correlation between greenhouse gas trends or soil redox status (as measured by percent paint removed from IRIS tubes) and functional gene composition, scaled by magnitude of correlation (using envfit).

Figure 6

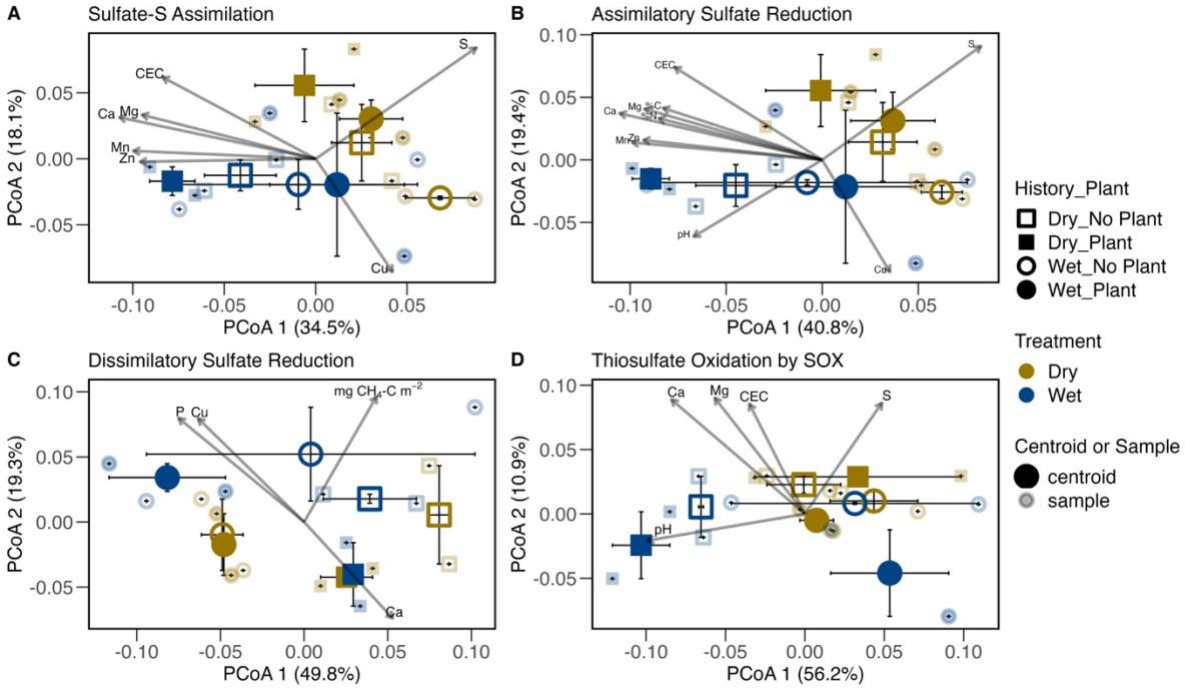

Figure 6. Ordination of sulfur functional gene modules after the 8-week experiment. Ordinations are based on principal coordinates analysis (PCoA), depicting community composition, at the end of the 8-week experiment, of the functional gene modules Sulfate-Sulfur Assimilation (M00616) (A), Assimilatory Sulfate Reduction (M00176) (B), Dissimilatory Sulfate Reduction (M00596) (C), and Thiosulfate Oxidation by SOX Complex (M00595) (D). Percent variation explained by each axis is listed in parentheses. Colors refer to hydrologic treatments, where brown = dry, dark blue = wet. Shapes refer to hydrologic history of the sample, where square = dry, circle = wet. The shape fill represents plant treatment, where open symbol = no plant, closed symbol = plant. Vectors represent significant ($P < 0.05$) correlation between greenhouse gas trends or soil physicochemical parameters, and functional gene composition, scaled by magnitude of correlation (using envfit).

Figure 7

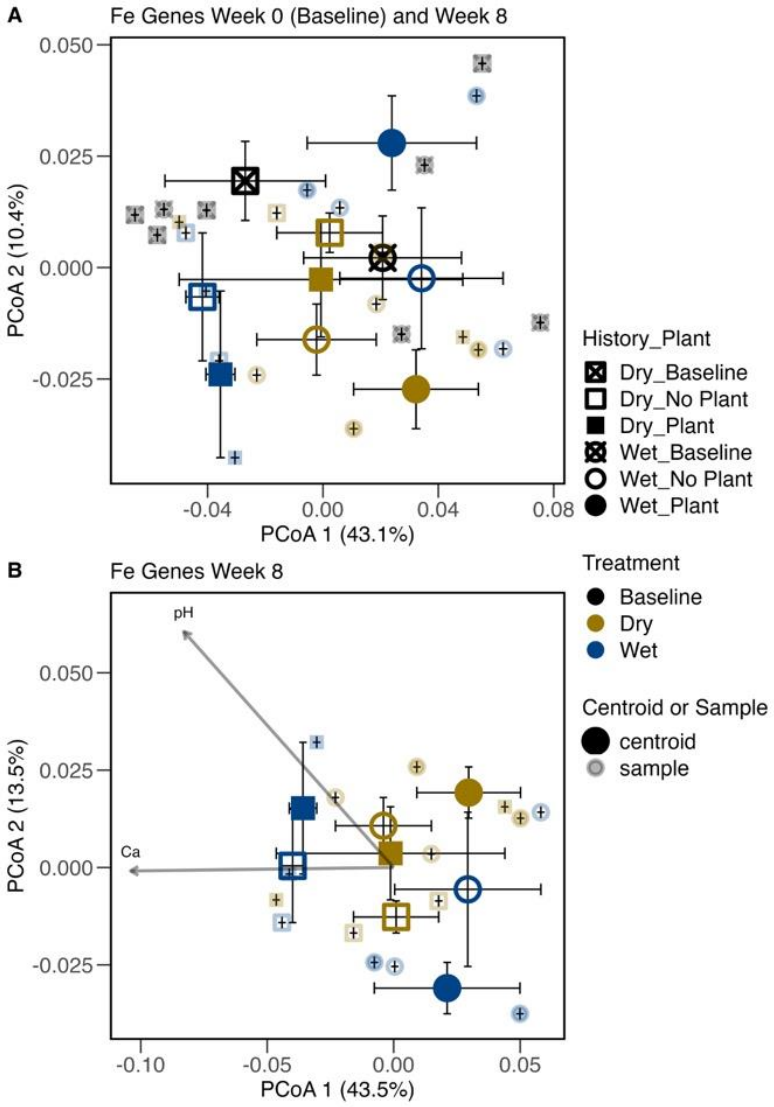

Figure 7. Ordination of iron functional gene composition. Ordinations are based on principal coordinates analysis (PCoA), depicting community composition of the functional gene modules: all Fe genes, as identified by FeGenie, at start and end of experiment (A), and all Fe genes envfit with greenhouse gases and soil physicochemical data from end of experiment (B). Percent variation explained by each axis is listed in parentheses. Colors refer to hydrologic treatments, where black = baseline, brown = dry, dark blue = wet. Shapes refer to hydrologic history of the sample, where square = dry, circle = wet. The shape fill represents plant treatment, where 'x' through symbol = baseline, open symbol = no plant, closed symbol = plant. Baseline samples were collected before the start of hydrologic and plant treatments and treatment samples collected after eight weeks. Vectors represent significant ($P < 0.05$) correlation between greenhouse gas trends or soil physicochemical parameters, and functional gene composition, scaled by magnitude of correlation (using envfit).

Figure 8

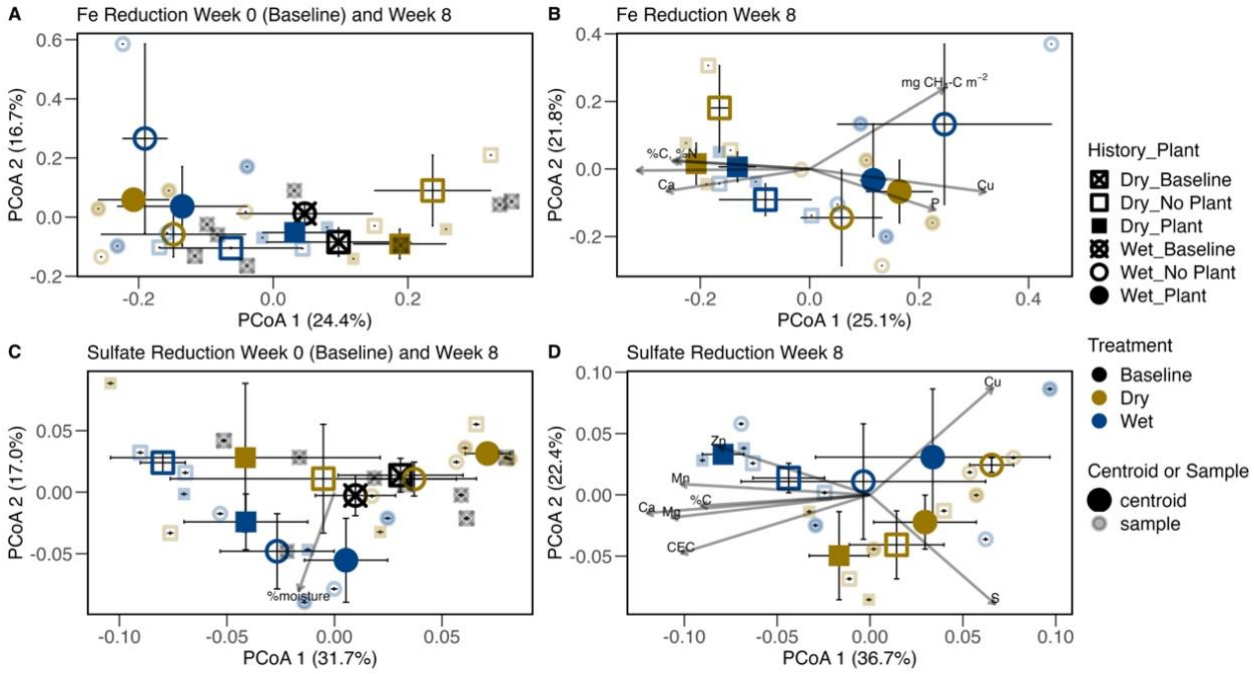

Figure 8. Ordination of iron reduction and sulfur reduction genes. Ordinations are based on principal coordinates analysis (PCoA), depicting community composition of the functional gene modules Fe reduction genes, identified by FeGenie, at Week 0 and Week 8 of the 8-week experiment (A), Fe reduction genes, identified by FeGenie, at end of 8-week experiment (B), sulfate reduction genes (both assimilatory and dissimilatory) at Week 0 and Week 8 of 8-week experiment (C), and sulfate reduction genes (both assimilatory and dissimilatory) at end of 8-week experiment (D). Percent variation explained by each axis is listed in parentheses. Colors refer to hydrologic treatments, where black = baseline, brown = dry, dark blue = wet. Shapes refer to hydrologic history of the sample, where square = dry, circle = wet. The shape fill represents plant treatment, where 'x' through symbol = baseline, open symbol = no plant, closed symbol = plant. Baseline samples were collected before the start of hydrologic and plant treatments and treatment samples were collected after eight weeks. Vectors represent significant ($P < 0.05$) correlation

between greenhouse gas trends or soil physicochemical parameters, and functional gene composition, scaled by magnitude of correlation (using envfit).

Table 1. Soil chemical and physical properties measured after eight weeks of hydrologic manipulation. Average (mean ± standard deviation) by hydrologic treatment and plant status reported. Abbreviations: MDL = Below detection limit.

HISTORY	DRY		INTERIM (DRY/WET)		WET	
Plant	No Plant	Plant	No Plant	Plant	No Plant	Plant
Moisture (%)	39 ± 0.31	14 ± 0.03	19 ± 0.16	13 ± 0.02	29 ± 0.23	62 ± 0.07
pH	5.31 ± 0.11	5.31 ± 0.09	5.4 ± 0.16	5.35 ± 0.1	5.55 ± 0.15	5.41 ± 0.17
NH_4^+ mg/L	0.39 ± 0.07	0.27 ± 0.04	0.26 ± 0.1	0.19 ± 0.02	0.77 ± 0.76	0.39 ± 0.42
NO_3^- mg/L	0.08 ± 0.07	MDL	0.25 ± 0.38	MDL	0.01 ± 0.0005	MDL
Total C (%)	4.63 ± 0.78	4.63 ± 0.81	4.48 ± 0.32	4.37 ± 0.52	4.91 ± 0.92	4.68 ± 0.74
Total N (%)	0.22 ± 0.03	0.22 ± 0.03	0.22 ± 0.01	0.21 ± 0.03	0.24 ± 0.04	0.23 ± 0.03
P ppm	21.00 ± 4.14	20.41 ± 4.4	23.58 ± 8.87	22.83 ± 8.37	23.16 ± 5.98	23 ± 5.79
K ppm	33.66 ± 5.97	30.25 ± 10.31	39.5 ± 11.44	26.75 ± 3.04	46.16 ± 16.02	34.25 ± 10.78
Mg ppm	77.58 ± 6.46	74.66 ± 11.43	86 ± 22.33	78.66 ± 16.47	89.25 ± 16.85	79.41 ± 18.8
S ppm	15.75 ± 1.94	15.33 ± 2.29	13.25 ± 1.25	12.16 ± 0.40	11.33 ± 1.21	11.5 ± 1.00
Fe ppm	252.66 ± 14.45	243.66 ± 17.06	275.33 ± 27.07	251.16 ± 37.6	306.83 ± 22.52	280.66 ± 40.71
Mn ppm	3.91 ± 1.15	3.41 ± 0.97	4.33 ± 1.16	4.58 ± 1.31	5.83 ± 1.32	5.58 ± 2.05
Humic matter (%)	2.35 ± 0.19	2.17 ± 0.14	2.04 ± 0.29	2.28 ± 0.22	1.98 ± 0.422	1.96 ± 0.43

Table 2. Summary of metagenome bins. Binning was performed using the IMG pipeline (MetaBAT, CheckM, GTDB, GTDB-tk). Bins are accessible at https://img.jgi.doe.gov/, under the Bin ID.

Bin ID	History	Treatment	Plant Presence/Absence	Bin Quality	Bin Lineage	GTDBTK Lineage	Bin Completeness	Bin Contamination	Total Number of Bases	Gene Count	Scaffold Count
3300036865_5	Dry	Baseline	Baseline	MQ	Bacteria; Proteobacteria; Betaproteobacteria; Burkholderiales	Bacteria; Proteobacteria; Gammaproteobacteria; Betaproteobacteriales; Burkholderiaceae; JOSHI-001	88.02	6.17	4674782	4849	502
3300036991_3	Dry	Baseline	Baseline	HQ	Bacteria; Proteobacteria; Gammaproteobacteria; Xanthomonadales; Rhodanobacteraceae; Dyella	Bacteria; Proteobacteria; Gammaproteobacteria; Xanthomonadales; Rhodanobacteraceae; Dyella	98.45	2.71	4930595	4528	168
3300036991_4	Dry	Baseline	Baseline	MQ	Bacteria; Proteobacteria; Alphaproteobacteria; Hyphomicrobiales	Bacteria; Proteobacteria; Alphaproteobacteria; Rhizobiales; Xanthobacteraceae	54.51	1.92	2325436	2615	451
3300036870_7	Dry	Wet	Plant	MQ	Archaea; Thaumarchaeota; unclassified; unclassified; unclassified; Candidatus Nitrosotalea; Candidatus Nitrosotalea devanaterra	Archaea; Crenarchaeota; Nitrososphaeria; Nitrososphaerales; Nitrosopumilaceae; Nitrosotalea	61	0.97	780222	1032	140
3300036873_3	Dry	Wet	No Plant	HQ	Bacteria	Bacteria; Bacteroidota; Kapabacteria	96.98	1.64	3157872	2807	109
3300036867_3	Wet	Baseline	Baseline	MQ	Bacteria; Proteobacteria;	Bacteria; Proteobacteria; Gammaproteobacteria; Betaproteobacteriales;	76.88	0.7	3880859	4065	463

					Betaproteobacteria; Burkholderiales	Burkholderiaceae; JOSHI-001					
3300036989_2	Wet	Baseline	Baseline	MQ	Bacteria; Proteobacteria; Alphaproteobacteria; Hyphomicrobiales	Bacteria; Proteobacteria; Alphaproteobacteria; Rhizobiales; Xanthobacteraceae; Pseudorhodoplanes	62.92	8.67	3626868	4149	720
3300036989_4	Wet	Baseline	Baseline	MQ	Bacteria; Actinobacteria; Thermoleophilia	Bacteria; Actinobacteriota; Thermoleophilia; Solirubrobacterales; 70-9; 70-9	80.23	5.11	2422891	2808	415
3300036990_3	Wet	Baseline	Baseline	MQ	Bacteria	Bacteria; Verrucomicrobiota; Verrucomicrobiae; Chthoniobacterales; UBA10450; UBA10450	61.4	0.72	2180017	2388	284
3300036875_5	Wet	Dry	Plant	MQ	Bacteria; Actinobacteria; Actinomycetia	Bacteria; Actinobacteriota; Actinobacteria; Streptosporangiales	51.1	8.78	3331403	3616	726
3300036898_4	Wet	Dry	Plant	MQ	Bacteria; Chloroflexi; Ktedonobacteria	Bacteria; Chloroflexota; Ktedonobacteria; Ktedonobacterales; Ktedonobacteraceae; UBA11361	85.26	1.98	4109904	4252	599
3300036898_5	Wet	Dry	Plant	MQ	Bacteria	Bacteria; Gemmatimonadota; Gemmatimonadetes; Gemmatimonadales; Gemmatimonadaceae	64.48	6.41	3359397	3472	616
3300036872_8	Wet	Wet	Plant	MQ	Bacteria	Bacteria; Nitrospirota; Thermodesulfovibrionia; Thermodesulfovibrionales	56.04	0.36	1448797	1708	290
3300036993_3	Wet	Wet	No Plant	MQ	Bacteria	Bacteria; Verrucomicrobiota; Verrucomicrobiae; Chthoniobacterales; UBA10450; UBA10450	74.22	4.2	3077671	3555	534

Abbreviations: MQ = medium quality, HQ = high quality

SUPPLEMENTAL FIGURES AND TABLES

Figure S1

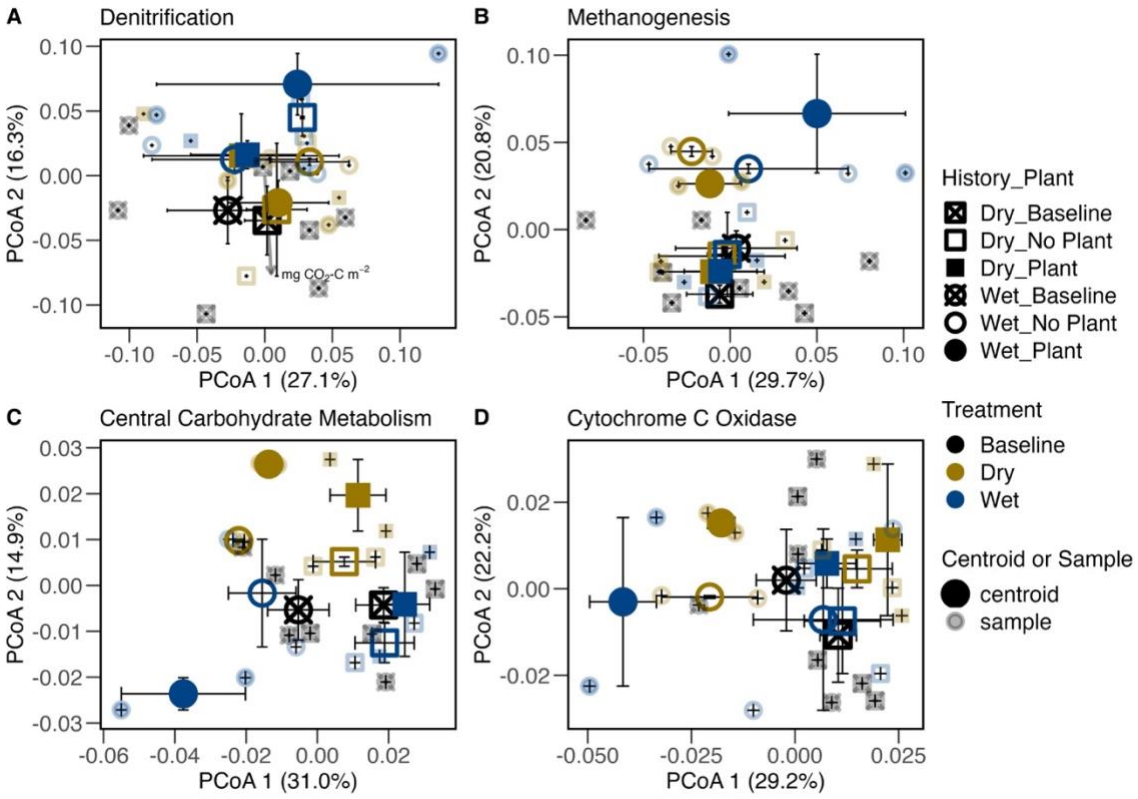

Figure S1. Ordination of carbon and nitrogen functional gene modules. Ordinations are based on principal coordinates analysis (PCoA), depicting community composition of the functional gene modules Denitrification (KEGG Module M00529) (A), Methanogen (M00617) (B), Central Carbohydrate Metabolism (M00001-M00011, M00307-M00309, M00580, and M00633) (C), and Prokaryotic Cytochrome C Oxidase (M00155) (D). Percent variation explained by each axis is listed in parentheses. Colors refer to hydrologic treatments, where black = baseline, brown = dry, dark blue = wet. Shapes refer to hydrologic history of the sample, where square = dry, circle = wet. The shape fill represents plant treatment, where 'x' through symbol = baseline, open symbol

= no plant, closed symbol = plant. Baseline samples were collected before the start of hydrologic and plant treatments and treatment samples were collected after eight weeks. Vectors represent significant ($P < 0.05$) correlation between greenhouse gas trends or soil redox status (as measured by percent paint removed from IRIS tubes) and functional gene composition, scaled by magnitude of correlation (using envfit). Modified versions of these figures were presented in Bledsoe et al. 2023 biorxiv.

Figure S2

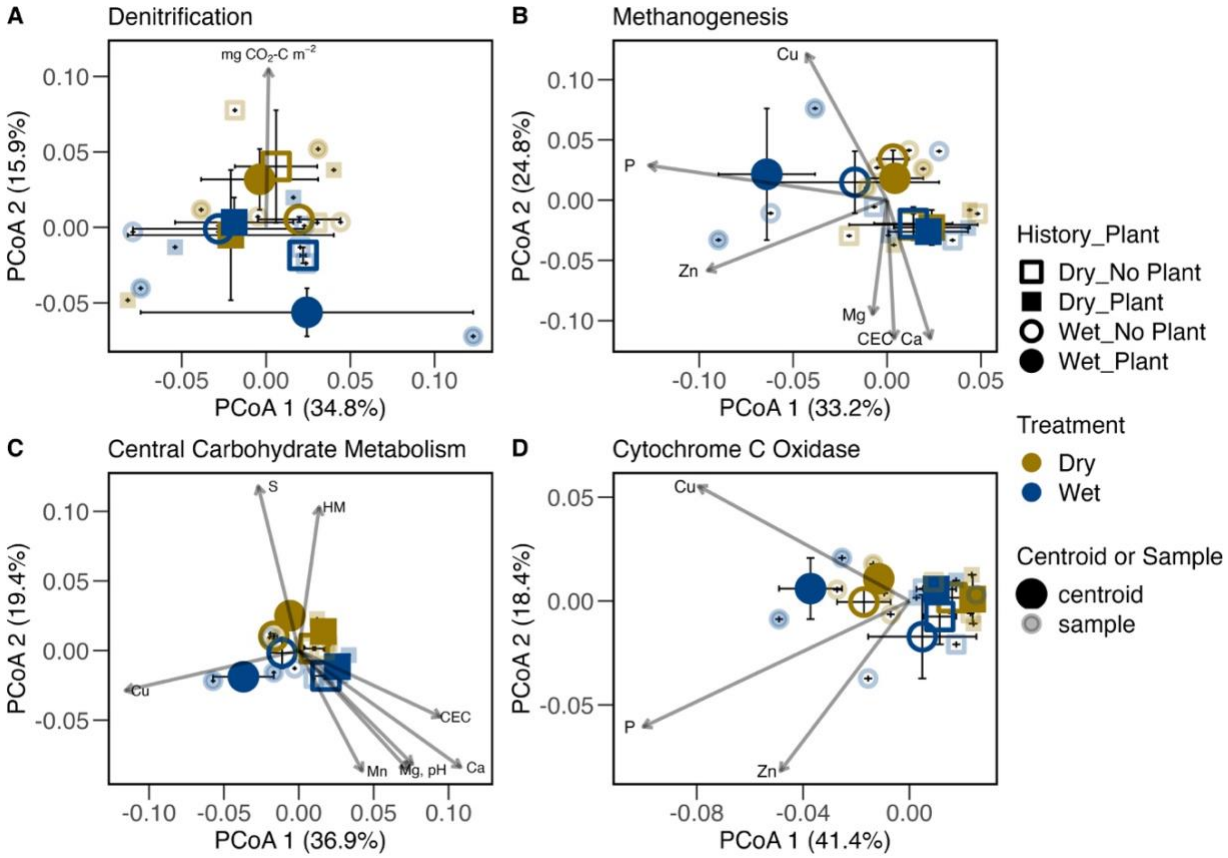

Figure S2. Ordination of carbon and nitrogen functional gene modules after the 8-week experiment. Ordinations are based on principal coordinates analysis (PCoA), depicting community composition of the functional gene modules, at the end of the 8-week experiment, of Denitrification (KEGG Module M00529) (A), Methanogen (M00617) (B), Central Carbohydrate Metabolism (M00001-M00011, M00307-M00309, M00580, and M00633) (C), and Prokaryotic Cytochrome C Oxidase (M00155) (D). Percent variation explained by each axis is listed in parentheses. Colors refer to hydrologic treatments, where brown = dry, dark blue = wet. Shapes refer to hydrologic history of the sample, where square = dry, circle = wet. The shape fill represents plant treatment, where open symbol = no plant, closed symbol = plant. Vectors represent significant ($P < 0.05$) correlation between greenhouse gas trends or soil physicochemical parameters, and functional gene composition, scaled by magnitude of correlation (using envfit).

Modified versions of these figures were presented in Bledsoe et al. 2023 biorxiv (Bledsoe et al., 2023).

Table S1. Mantel test for correlation among paired Bray-Curtis distance matrices of functional gene modules. The Mantel Statistic (R) is based on Pearson's product-moment correlation. Bold text indicates significant correlations ($P < 0.05$).

X Distance Matrix	Y Distance Matrix	Mantel Statistic R	P-value
Fe Reduction (FeGenie)	SO_4^{2-} Reduction (Assimilatory and Dissimilatory)	0.064	0.249
Fe Reduction (FeGenie)	**Assimilatory SO_4^{2-} Reduction**	**0.222**	**0.008**
Fe Reduction (FeGenie)	**Dissimilatory SO_4^{2-} Reduction**	**0.313**	**0.006**
Denitrification	Thiosulfate Oxidation by SOX Complex	0.117	0.170
DNRA	**Thiosulfate Oxidation by SOX Complex**	**0.196**	**4.990e-2**

Abbreviations. SOX: thiosulfate oxidizing multienzyme complex, DNRA: dissimilatory nitrate reduction to ammonium

Table S2. Hydrology-specific Mantel test for correlation among paired Bray-Curtis distance matrices of functional gene modules. The Mantel Statistic (R) is based on Pearson's product-moment correlation. Distance matrices were subset according to wet history, dry history, wet treatment, and dry treatment. Mantel Tests were then performed on sulfate reduction and Fe reduction distance matrices in each respective hydrologic condition, e.g., wet history. Bold text indicates significant correlations ($P < 0.05$).

X Distance Matrix	Y Distance Matrix	Wet History	Dry History	Wet Treatment	Dry Treatment
Sulfate Reduction	Iron Reduction	R = 0.148, P = 0.214	R = 0.010, P = 0.446	**R = 0.360, P = 0.010**	R = -0.166, P = 0.728

Table S3. Summary of distance-based partial least squares regression. The adjusted (adj) R^2 represents how much variation in GHG concentration is explained (%) by each component (Comp) derived from functional gene composition, 16S rRNA gene composition, or soil properties distance matrix.

GHG ~ distance matrix	Time point	Comp	Comp 1	Comp 2	Comp 3	Comp 4	Comp 5	Comp 6
N_2O ~ Denitri-fication	Week 0	R^2	41.3	72.9	87.5	92.9	98.8	99.9
		adj R^2	31.6	62.0	78.2	83.4	95.7	99.5
		gvar	48.2	66.3	79.5	88.3	91.2	97.9
		crit	7.69e-5	4.84e-5	3.21e-5	2.86e-5	8.71e-6	1.43e-6
N_2O ~ Denitri-fication	Week 8	R^2	76.2	79.1	82.9	86.6	91.0	94.1
		adj R^2	74.5	75.9	78.6	81.8	86.5	90.1
		gvar	9.09	44.0	64.9	83.3	87.4	91.3
		crit	1.98e-3	1.99e-3	1.89e-3	1.73e-3	1.39e-3	1.10e-3
CH_4 ~ Methanogene sis	Week 0	R^2	57.0	76.9	94.9	98.7	99.9	1.00e2
		adj R^2	49.9	67.6	91.1	97.0	99.6	99.7
		gvar	44.7	71.4	80.4	89.6	93.3	97.4
		crit	69.0	50.6	16.0	6.26	0.969	0.720
CH_4 ~ Methanogene sis	Week 8	R^2	23.1	37.8	70.7	78.2	93.6	96.7
		adj R^2	17.7	28.3	63.4	70.2	90.4	94.6
		gvar	30.2	59.7	68.5	81.8	84.1	88.7
		crit	16.2	15.0	8.22	7.18	2.50	1.55
CO_2 ~ Central Carbohydrate Metabolism	Week 0	R^2	76.2	99.2	99.9	1.00e2	1.00e2	1.00e2
		adj R^2	72.3	98.9	99.8	1.00e2	1.00e2	1.00e2
		gvar	44.6	60.6	66.7	76.6	81.8	90.9
		crit	9.24	0.418	0.0956	0.0180	2.47e-4	1.19e-5
CO_2 ~ Central Carbohydrate Metabolism	Week 8	R^2	44.1	80.1	85.5	92.0	98.1	99.6
		adj R^2	40.1	77.0	81.9	89.1	97.1	99.3
		gvar	22.4	28.4	62.4	76.0	80.6	84.4
		crit	25.1	10.3	8.67	5.62	1.60	0.433
CO_2 ~ Cytochrome C Oxidase	Week 0	R^2	49.3	94.8	97.8	99.6	99.8	1.00e2
		adj R^2	40.9	92.8	96.2	99.1	99.4	99.7
		gvar	75.1	87.9	96.6	97.4	98.8	99.4

		crit	19.7	2.73	1.64	0.459	0.392	0.211
CO_2 ~ Cytochrome C Oxidase	Week 8	R^2	13.0	17.1	28.8	41.9	54.6	60.6
		adj R^2	6.78	4.39	11.0	20.8	31.9	34.3
		gvar	28.3	76.5	84.7	89.2	93.5	98.1
		crit	39.1	42.8	42.6	40.8	40.0	39.9
N_2O ~ 16S rRNA gene	Week 8	R^2	27.4	41.6	71.3	87.8	92.9	97.0
		adj R^2	25.2	38.0	68.6	86.2	91.7	96.3
		gvar	10.1	36.8	49.4	56.9	66.4	71.2
		crit	1.58e-3	1.35e-3	7.04e-4	3.19e-4	1.98e-4	9.05e-5
CH_4 ~ 16S rRNA gene	Week 8	R^2	22.6	54.0	82.2	94.1	96.8	99.4
		adj R^2	20.4	51.2	80.6	93.4	96.3	99.3
		gvar	28.3	44.3	52.3	57.8	65.9	69.1
		crit	3.10	1.96	0.802	0.281	0.163	0.0326
CO_2 ~ 16S rRNA gene	Week 8	R^2	19.5	38.3	59.2	86.0	93.8	96.6
		adj R^2	17.1	34.6	55.4	84.2	92.8	95.9
		gvar	29.0	45.6	53.8	58.7	66.0	72.2
		crit	14.4	11.7	8.20	3.00	1.40	0.832
N_2O ~ soil parameters	Week 8	R^2	12.2	22.6	28.6	42.7	54.0	65.5
		adj R^2	9.60	17.9	21.9	35.3	46.3	58.3
		gvar	37.0	63.8	73.4	77.2	81.6	84.5
		crit	1.92e-3	1.79e-3	1.75e-3	1.50e-3	1.28e-3	1.03e-3
CH_4 ~ soil parameters	Week 8	R^2	13.3	34.0	64.2	76.7	92.8	96.5
		adj R^2	10.8	30.0	60.8	73.7	91.6	95.7
		gvar	49.6	65.4	70.6	76.5	78.8	81.4
		crit	3.48	2.81	1.62	1.12	0.369	0.194
CO_2 ~ soil parameters	Week 8	R^2	12.5	35.5	45.5	51.6	58.2	66.5
		adj R^2	9.97	31.6	40.4	45.4	51.2	59.5
		gvar	52.6	60.1	64.5	72.1	80.5	84.8
		crit	15.6	12.2	11.0	10.4	9.53	8.16

Abbreviations are GHG, greenhouse gas; adj, adjusted; gvar, total weighted geometric variability; crit, value of criterion defined in method.

Table S4. Summary of select iron and sulfur gene modules related to greenhouse gases, using distance-based partial least squares regression. The adjusted (adj) R^2 represents how much variation in GHG concentration is explained (%) by each component (Comp) derived from functional gene composition. Selected pairings of gene modules and GHGs is based on significant ($P < 0.05$) relationships identified between PCoAs of gene modules and GHGs, using envfit.

GHG ~ Gene Module	Timepoint	Total Components (n – 1)	Component	Comp 1	Comp 2
CO_2 ~ Assimilatory SO_4^{2-} Reduction	Week 0	7	R^2	60.74	87.752
			adj R^2	54.19	82.853
			gvar	43.75	69.768
			crit	15.26	6.478
CO_2 ~ Assimilatory SO_4^{2-} Reduction	Week 8	15	R^2	28.58	37.84
			adj R^2	23.47	28.28
			gvar	58.13	77.50
			crit	32.13	32.10
CH_4 ~ Dissimilatory SO_4^{2-} Reduction	Week 0	7	R^2	28.40	50.43
			adj R^2	16.47	30.60
			gvar	67.30	81.84
			crit	115.05	108.43
CH_4 ~ Dissimilatory SO_4^{2-} Reduction	Week 8	15	R^2	51.26	66.840
			adj R^2	47.78	61.738
			gvar	49.51	85.747
			crit	10.27	8.022
CH_4 ~ Fe Reduction	Week 0	7	R^2	12.423	56.77
			adj R^2	-2.173	39.48
			gvar	61.198	69.80
			crit	140.729	94.55
CH_4 ~ Fe Reduction	Week 8	15	R^2	74.439	88.863
			adj R^2	72.613	87.150
			gvar	41.809	54.740
			crit	5.386	2.694

Abbreviations are GHG, greenhouse gas; adj, adjusted; gvar, total weighted geometric variability; crit, value of criterion defined in method; comp, component.

Table S5. Summary of permutational multivariate analysis of variance. The models include baseline samples and compare microbial functional composition due to main effects (plant, hydrologic history, hydrologic treatment) and interaction between plant × history and plant × treatment. Bold text indicates significant differences ($P < 0.05$).

Functional Gene Module	Main Effect	DF	SumSq	R^2	F	P-value
Denitrification	Plant	2	0.010	0.086	0.840	0.576
	History	1	2.6e-5	2.4e-4	-0.005	0.991
	Treatment	1	0.004	0.034	0.667	0.623
	Plant × History	2	0.004	0.040	0.386	0.934
	Plant × Treatment	1	0.002	0.016	0.309	0.887
Methanogenesis	Plant	2	0.006	0.085	1.045	0.402
	History	1	**0.011**	**0.154**	**3.795**	**0.007**
	Treatment	1	0.004	0.048	1.184	0.315
	Plant × History	2	0.003	0.042	0.515	0.870
	Plant × Treatment	1	0.002	0.024	0.586	0.697
Central Carbohydrate Metabolism	Plant	2	0.002	0.067	0.998	0.423
	History	1	**0.006**	**0.211**	**6.262**	**9.999e-5**
	Treatment	1	**0.003**	**0.092**	**2.735**	**0.012**
	Plant × History	2	0.002	0.054	0.803	0.693
	Plant × Treatment	1	0.001	0.036	1.065	0.360
Cytochrome C Oxidase	Plant	2	0.001	0.076	1.211	0.316
	History	1	**0.002**	**0.227**	**7.224**	**0.001**
	Treatment	1	3.070e-4	0.031	0.977	0.418
	Plant × History	2	0.001	0.087	1.388	0.250
	Plant × Treatment	1	0.001	0.078	2.491	0.081
	Plant	2	0.006	0.066	0.891	0.527

Sulfate-Sulfur Assimilation	History	1	0.005	0.061	1.654	0.153
	Treatment	1	**0.013**	**0.144**	**3.917**	**0.008**
	Plant × History	2	0.008	0.090	1.228	0.276
	Plant × Treatment	1	0.004	0.051	1.389	0.222
Assimilatory Sulfate Reduction	Plant	2	0.006	0.066	0.872	0.514
	History	1	0.004	0.046	1.221	0.288
	Treatment	1	**0.015**	**0.156**	**4.111**	**0.013**
	Plant × History	2	0.009	0.091	1.193	0.307
	Plant × Treatment	1	0.003	0.031	0.817	0.497
Dissimilatory Sulfate Reduction	Plant	2	0.012	0.113	1.859	0.132
	History	1	**0.032**	**0.316**	**10.397**	**0.001**
	Treatment	1	0.003	0.029	0.947	0.388
	Plant × History	2	0.005	0.046	0.755	0.577
	Plant × Treatment	1	0.001	0.010	0.3171	0.784
Thiosulfate Oxidation by SOX Complex	Plant	2	0.004	0.045	0.608	0.637
	History	1	**0.022**	**0.243**	**6.547**	**0.009**
	Treatment	1	0.007	0.078	2.095	0.135
	Plant × History	2	0.002	0.017	0.234	0.939
	Plant × Treatment	1	0.002	0.024	0.656	0.501
Sulfate Reduction (combined assimilatory and dissimilatory)	Plant	2	0.007	0.060	0.786	0.619
	History	1	**0.012**	**0.108**	**2.830**	**0.030**
	Treatment	1	**0.013**	**0.111**	**2.906**	**0.026**
	Plant × History	2	0.009	0.077	1.016	0.418
	Plant × Treatment	1	0.004	0.034	0.879	0.476
Fe Genes (all)	Plant	2	0.001	0.028	0.315	0.880
	History	1	**0.006**	**0.185**	**4.173**	**0.031**
	Treatment	1	0.001	0.044	0.994	0.354
	Plant × History	2	0.001	0.028	0.318	0.872
	Plant × Treatment	1	2.01e-4	0.006	0.139	0.909

Fe Reduction (FeGenie)	Plant	2	0.157	0.094	1.189	0.280
	History	1	**0.221**	**0.132**	**3.358**	**0.004**
	Treatment	1	0.010	0.060	1.513	0.161
	Plant × History	2	0.102	0.061	0.772	0.700
	Plant × Treatment	1	0.038	0.023	0.580	0.787
Fe Reduction (TIGRFAMS mtrBC)	**Plant**	2	**0.032**	**0.335**	**9.967**	**0.002**
	History	1	0.004	0.037	2.187	0.162
	Treatment	1	**0.031**	**0.319**	**19.012**	**0.0002**
	Plant × History	2	0.003	0.036	1.058	0.367
	Plant × Treatment	1	4.66e-4	0.005	0.288	0.598
Dissimilatory Nitrate Reduction to Ammonium (DNRA)	Plant	2	0.014	0.115	1.282	0.270
	History	1	0.004	0.035	0.773	0.529
	Treatment	1	0.006	0.049	1.090	0.355
	Plant × History	2	0.009	0.079	0.881	0.518
	Plant × Treatment	1	0.001	0.007	0.156	0.951

Abbreviations are DF: degrees of freedom, SumSq: sum of squares

Table S6. Soil redox conditions and greenhouse gas concentrations linear regression. Bold text indicates significant differences ($P < 0.05$).

Greenhouse Gas	Formula	Residual Standard Error	Degrees of Freedom	Multiple R^2	Adjusted R^2	P-value
CH_4	log(CH_4) ~ redox status	**0.905**	**34**	**0.282**	**0.261**	**8.594e-4**
CH_4	log(CH_4, minus outlier) ~ redox status	**0.321**	**33**	**0.465**	**0.448**	**6.572e-6**
CO_2	log(CO_2) ~ redox status	**22.55**	**34**	**0.210**	**0.187**	**0.005**
N_2O	log(N_2O) ~ redox status	0.275	34	0.038	0.009	0.254

Figure S3.

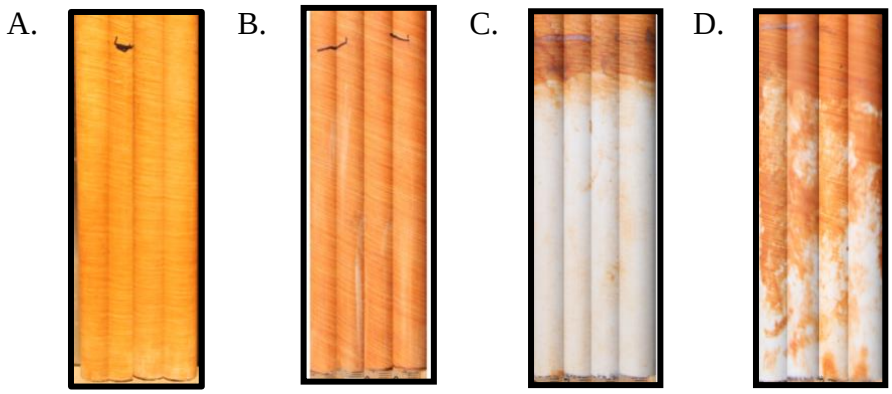

Figure S3. Indicator of Reduction in Soils (IRIS) tubes. Representative IRIS tubes collected from the dry hydrologic treatment without plants (A.) and with plants (B), wet treatment without plants (C), in wet treatment with plants (D).

Figure S4.

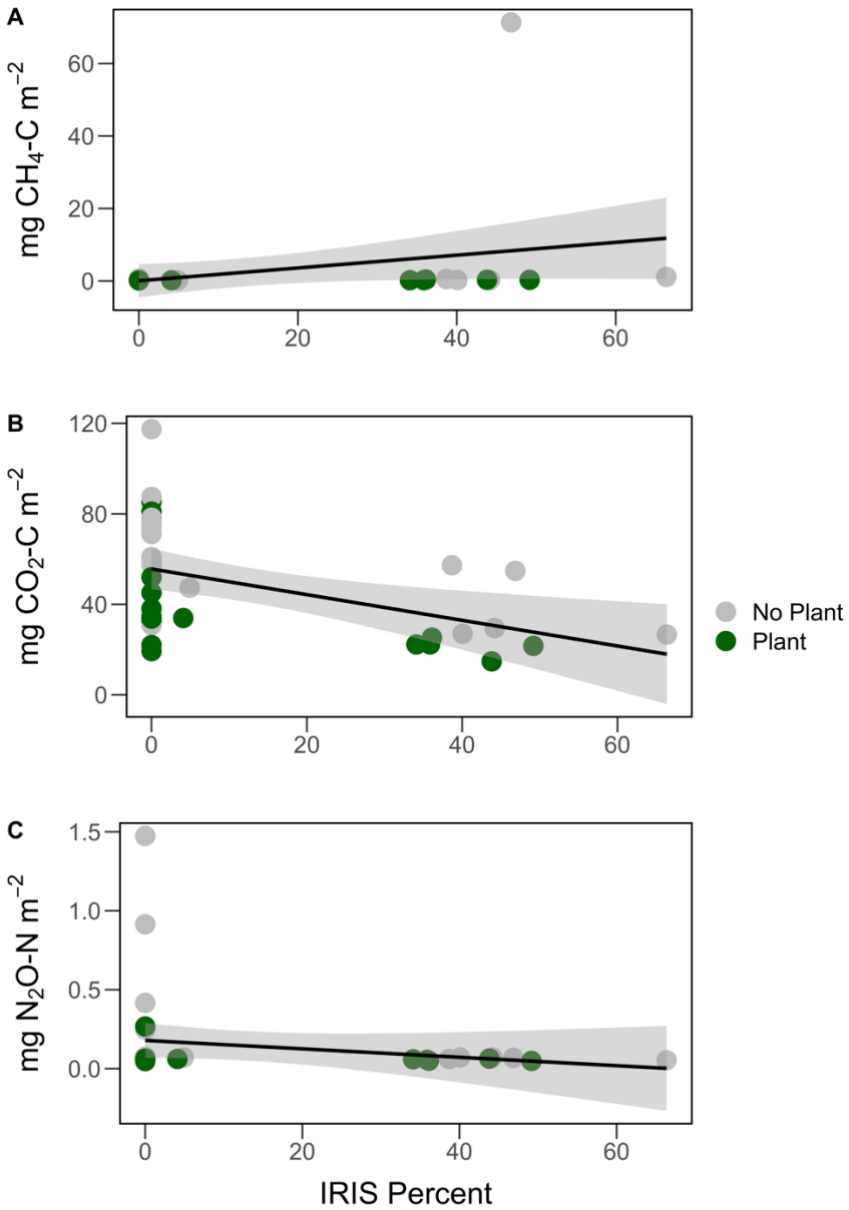

Figure S4. Soil redox status (IRIS percent) and greenhouse gas concentrations. IRIS (indicator of reduction in soils) percent is the percent of paint removed from IRIS tubes, an indicator of soil redox status. Concentrations of greenhouse gases: CH_4 (A), CO_2 (B), N_2O (C). Colors refer to vegetation treatment: grey = no plant, green = plant.

Figure S5.

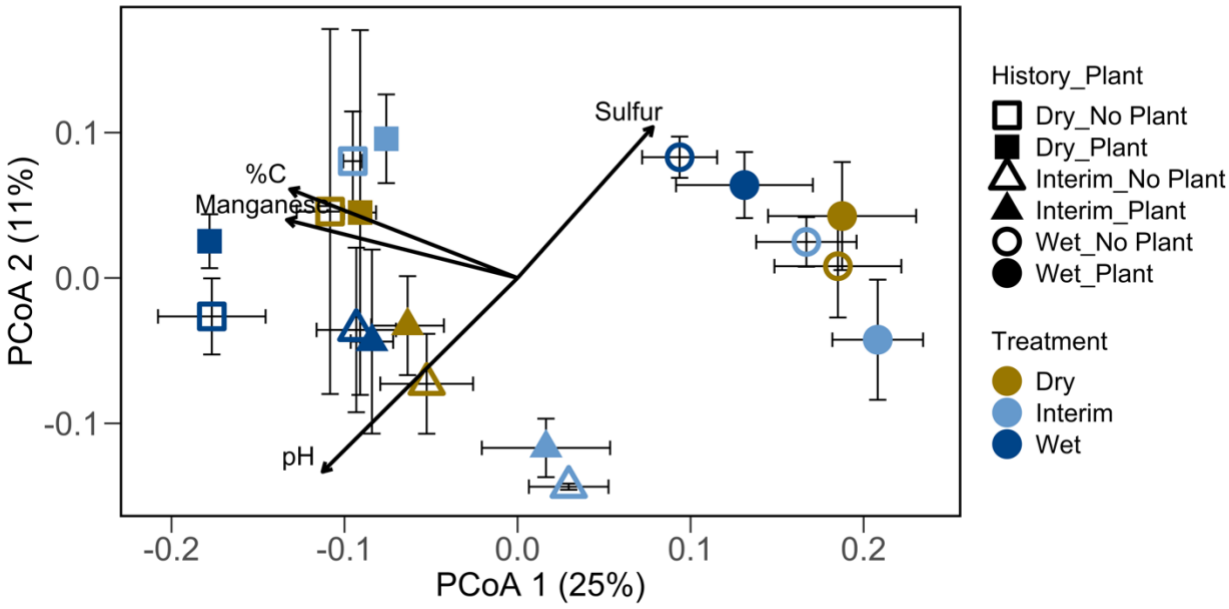

Figure S5. Ordination based on principal coordinates analysis (PCoA) depicting community composition of bacteria and archaea, based on the 16S rRNA gene. Percent variation explained by each axis is listed in parentheses. Colors refer to hydrologic treatments: brown = dry, light blue = interim, dark blue = wet. Shapes refer to hydrologic history of the sample: square = dry, triangle = interim, circle = wet. Open shapes refer to samples from mesocosms without plants, while closed shapes refer to samples from mesocosms with plants. Labelled vectors represent relationships among soil physiochemical variables and the microbial community ordination with $P \leq 0.05$, scaled by their correlation (using envfit). This figure was presented in Bledsoe et al. 2023.